

# Spatio-temporal characteristics of seasonal to multi-decadal variability of pCO<sub>2</sub> and air-sea CO<sub>2</sub> fluxes in the equatorial Pacific Ocean

Vinu K. Valsala<sup>1</sup>

Mathew Koll Roxy<sup>1</sup>

Karumuri Ashok<sup>2,1</sup>

Raghu Murtugudde<sup>3</sup>

<sup>1</sup> Indian Institute of Tropical Meteorology, Pune, India

<sup>2</sup> University of Hyderabad, Hyderabad, India

<sup>3</sup>University of Maryland, Maryland, USA

**Date: 18-Nov-2014**

Corresponding author address:

Dr. Vinu K. Valsala,  
Senior Scientist,  
Center for Advanced Training in Earth System Sciences (CAT-ESSC),  
Indian Institute of Tropical Meteorology, Pune, India.  
E-Mail: valsala@tropmet.res.in

This article has been accepted for publication and undergone full peer review but has not been through the copyediting, typesetting, pagination and proofreading process which may lead to differences between this version and the Version of Record. Please cite this article as  
doi: 10.1002/2014JC010212

© 2014 American Geophysical Union

Received: Jun 05, 2014; Revised: Nov 19, 2014; Accepted: Dec 04, 2014

## Abstract

Seasonal, interannual and multi-decadal variability of seawater pCO<sub>2</sub> and air-sea CO<sub>2</sub> fluxes in the equatorial Pacific Ocean for the past 45 years (1961 to 2005) are examined using a suite of experiments performed with an offline biogeochemical model driven by re-analysis ocean products. The processes we focus on are: (a) the evolution of seasonal cycle of pCO<sub>2</sub> and air-sea CO<sub>2</sub> fluxes during the dominant interannual mode in the equatorial Pacific, i.e., the El Niño-Southern Oscillation (ENSO), (b) its spatio-temporal characteristics, (c) the combined and individual effects of wind and ocean dynamics on pCO<sub>2</sub> and CO<sub>2</sub> flux variability and their relation to canonical (eastern Pacific) and central Pacific (Modoki) ENSOs and (d) the multi-decadal variability of carbon dynamics in the equatorial Pacific and its association with the Pacific Decadal Oscillations (PDO). The simulated mean and seasonal cycle of pCO<sub>2</sub> and CO<sub>2</sub> fluxes are comparable with the observational estimates and with other model results. A new analysis methodology based on the traditional Empirical Orthogonal Functions (EOF) applied over a time-time domain is employed to elucidate the dominant mode of interannual variability of pCO<sub>2</sub> and air-sea CO<sub>2</sub> fluxes at each longitude in the equatorial Pacific. The results show that the dominant interannual variability of CO<sub>2</sub> fluxes in the equatorial Pacific (averaged over 5°N-10°S) co-evolves with that of ENSO. Generally a reduced CO<sub>2</sub> source in the central-to-eastern equatorial Pacific evident during June-July of the El Niño year (Year:0) peaks through September of Year:0 to February of Year:+1 and recovers to a normal source thereafter. In the region between 160°W-110°W, the canonical El Niño controls the dominant variability of CO<sub>2</sub> fluxes (mean and RMS of anomaly from 1961 to 2005 is  $0.43 \pm 0.12 \text{ PgC yr}^{-1}$ ). However, in the western (160°E-160°W) and far eastern (110°W-90°W) equatorial Pacific, CO<sub>2</sub> flux variability is dominantly influenced by the El Niño-Modoki ( $0.3 \pm 0.06$  and  $0.11 \pm 0.04 \text{ PgC yr}^{-1}$ , respectively). On the other hand, the interannual variability of pCO<sub>2</sub> is correlated with the canonical El Niño mostly to the east of 140°W and with El Niño-Modoki to the west of 140°W. De-coupling of CO<sub>2</sub> flux and pCO<sub>2</sub> variability at various locations in the equatorial Pacific is attributable to the differences in the combined and individual effects of ocean dynamics and winds associated with these two types of ENSO.

A multi-decadal variability in the equatorial Pacific sea-air CO<sub>2</sub> fluxes and pCO<sub>2</sub> exhibits a positive phase during the 1960s, a negative phase during the 1980s, and then positive again by the 2000s. Within the ocean, the dissolved inorganic carbon (DIC) anomalies are traceable to the northern Pacific via thermocline pathways at decadal

Accepted Article

timescales. The multi-decadal variability of equatorial Pacific CO<sub>2</sub> fluxes and pCO<sub>2</sub> are determined by the phases of the PDO and the corresponding scale of the El Niño-Modoki variability, whereas canonical El Niño's contribution is to mainly determine the variability at interannual timescales. This study segregates the impacts of different types of ENSOs on the equatorial Pacific carbon cycle and sets the framework for analysing its spatio-temporal variability under global warming.

## 1. Introduction

The tropical belt of the ocean acts as a source of carbon dioxide ( $\text{CO}_2$ ) to the atmosphere with an annual mean emission of approximately  $0.64 \pm 0.22$  peta grams carbon in the present decade [1 peta =  $10^{15}$ ; Ishii et al., 2014, Landschützer et al., 2014, Fay and McKinley, 2013, Sarma et al., 2013, Schuster et al., 2013, Gruber et al., 2009, Takahashi et al., 2009, Feely et al., 2006]. Among the tropical oceans, the Pacific alone can account for a majority of this emission ( $\sim 0.44 \pm 0.14 \text{ PgC yr}^{-1}$ ) while exhibiting large scale spatial and temporal variability in the surface ocean  $\text{pCO}_2$  (partial pressure of  $\text{CO}_2$ ), air-sea  $\text{CO}_2$  fluxes and other biological responses driven by the El Niño-Southern Oscillation (ENSO) [Ishii et al., 2014, Lee et al., 2014, Messie and Chavez, 2013, Radenac et al., 2012, Turk et al., 2011, Feely et al., 2006, 2002, Murtugudde et al., 1999]. The strong trade winds in the tropics converge into the Inter-Tropical Convergence Zone but drive an Ekman divergence and equatorial upwelling due to the change in sign of the Coriolis effect across the equator. The zonal and meridional Ekman transports and the associated upwelling lift the thermocline and generate a thermocline-mixed layer interaction, which is crucial for the ENSO dynamics. This upwelling also brings up deeper nutrient and carbon rich water to the surface and makes this zone a region of oceanic outgassing of  $\text{CO}_2$  as well as a venue for intense biological production [Chavez et al., 1999, Gierach et al., 2012] and also bio-physical feedbacks which play into ENSO dynamics [Murtugudde et al. 2002, Jochum et al. 2010]. This peculiar property of upwelling and enrichment of  $\text{CO}_2$  makes the equatorial Pacific a region where  $\text{pCO}_2$ -SST relation displays a negative slope in contrast to the expected tendency that  $\text{pCO}_2$  increases with SST [Feely et al., 2006, Cosca et al., 2003, Eitchoet al., 1999].

Takahashi et al., [2009] summarized the seasonal variability of global air-sea  $\text{CO}_2$  fluxes and  $\text{pCO}_2$  by synthesizing over 3 million observations of surface ocean  $\text{pCO}_2$ . The surface ocean  $\text{pCO}_2$  based estimates show that the eastern tropical Pacific (east of  $160^{\circ}\text{W}$  and within  $18^{\circ}\text{N}-18^{\circ}\text{S}$ ) is a source of  $\text{CO}_2$  with a magnitude of  $0.45 \text{ PgC yr}^{-1}$  [Ishii et al., 2014]. The emission is strongest during June to September when the SST is typically at its seasonal minimum [Takahashi et al., 2009, Ishii et. al., 2014]. On the other hand, the western tropical Pacific (west of  $160^{\circ}\text{W}$ ,  $18^{\circ}\text{N}-18^{\circ}\text{S}$ ) is a mild source of  $\text{CO}_2$  with an annual mean emission of  $0.06 \text{ PgC yr}^{-1}$  [Ishii et al., 2014].

The major interannual variability in this region is driven by ENSO. The central to eastern equatorial Pacific is a strong source of CO<sub>2</sub> during La Niña events, near neutral during strong El Niños, and a weak source during weak El Niños [Feely et al., 1995, 1997 and 1999]. El Niño induced convergence in the central and eastern equatorial Pacific suppresses the upwelling of CO<sub>2</sub> rich water causing a reduction in the surface ocean carbon content. In addition, the dissolved inorganic carbon (DIC) depleted water is advected in from the western Pacific to the central and eastern Pacific [Picaut et al., 1997] during an El Niño causing a reduction in oceanic pCO<sub>2</sub> [Cosca et al., 2003]. An empirical estimate of the pCO<sub>2</sub> within 165°E-95°W, 5°N-10°S, based on the pCO<sub>2</sub>-SST relationship shows a maximum reduction of ~25 μatm in oceanic pCO<sub>2</sub> during the 1982-83 El Niño and ~40 μatm during the 1997-98 El Niño compared to the normal ambient values [Feely et al., 2006, Figure 8b]. CO<sub>2</sub> fluxes from central and eastern equatorial Pacific during the mature phase of 1997-98 El Niño reduced to  $0.2 \pm 0.15$  moles m<sup>-2</sup> yr<sup>-1</sup> and after the recovery from El Niño, these values surged to 2~6 moles m<sup>-2</sup> yr<sup>-1</sup> [Chavez et al., 1999].

Estimates made by inversions of the atmospheric CO<sub>2</sub> mole fraction data suggest a peak-to-peak interannual variability of  $0.53 \pm 0.08$  PgC yr<sup>-1</sup> in the tropical Pacific and are consistent with the general consensus regarding the evolution of the CO<sub>2</sub> flux during El Niño years [Ishii et al., 2014, Gurney et al., 2004, Patra et al., 2005, McKinley et al., 2005, Gruber et al., 2009, Fay and McKinley, 2013]. Park et al., [2010] utilized the SST-pCO<sub>2</sub> relations to empirically produce a three decade long global CO<sub>2</sub> flux product and reported a similar ENSO-CO<sub>2</sub> flux relationship.

On the other hand, Takahashi et al. [2003] and its extension by Feely et al. [2006] highlight a decadal signal (from 1980s to 2000s) in the equatorial Pacific fCO<sub>2</sub> (fugacity of CO<sub>2</sub>) in the observations made during the TAO array service cruises. The authors conclude that during the pre-1990 period, fCO<sub>2</sub> is nearly unchanged or slightly decreases with time, whereas it increases after 1990 at rates similar to or exceeding the atmospheric CO<sub>2</sub> growth rate. In addition, there has been an increase (~27%) in the outgassing of CO<sub>2</sub> after the 1997-98 climate regime shift seen as a phase change in the Pacific Decadal Oscillation (PDO) and the related increase in wind speeds [Feely et al., 2006].

A similar decadal signal is found in the ocean DIC data from the north Pacific [Sabine et al., 2008] and in the primary production data from the equatorial Pacific [Friedrichs et al., 2009]. The decadal increase in the DIC and apparent oxygen utilization (AOU) observed in the north Pacific are larger than those expected from the anthropogenic inputs alone. Presumably, they are driven by decadal changes in the ocean circulation [Sabine et al., 2008]. Ishii et al., [2009] identified decadal variability in the western Pacific warm-pool DIC data and suggested that they are broadly consistent with the variability in geostrophic convergence in the tropical-to-subtropical Pacific.

### 1a. Modelling studies

A number of modelling studies have focused on simulating the interannual variability of ocean pCO<sub>2</sub> and air-sea CO<sub>2</sub> fluxes of the global ocean [Obata and Kitamura, 2003, Le Quere et al. 2000, 2003, McKinley et al., 2004, Li and Xu., 2013, Jones et al., 2001] and other biological responses driven by ENSO [Christian et al., 2002, Wang et al. 2005, 2006a, b, Picaut et al., 2001]. These studies concluded that the net rate of change of pCO<sub>2</sub> in the equatorial Pacific on interannual time-scales, to a large extent (i.e., over ~60%) is accounted for by the variability induced due to DIC dynamics alone. These earlier studies also concluded that the tropical Pacific accounts for ~70% of the global oceanic CO<sub>2</sub> flux variability at interannual timescales. Ishii et al., [2014] provide a synthesized estimate of the mean and the interannual variability of tropical Pacific pCO<sub>2</sub>/CO<sub>2</sub> fluxes simulated by various biogeochemical models.

There is a handful of modelling studies to-date on the decadal and multi-decadal aspects of the Pacific carbon cycle but the spatio-temporal evolution of the variability in the equatorial Pacific Ocean has not been addressed in sufficient detail. Seferian et al., [2013] report global multi-decadal ocean pCO<sub>2</sub> and air-sea CO<sub>2</sub> fluxes and the associated mechanisms but focus mainly on the north Atlantic, north Pacific and the Southern Oceans. Valsala et al., [2012] proposed a mechanism by which PDO imprints its ‘four-polar’ structure in the north Pacific CO<sub>2</sub> fluxes and pCO<sub>2</sub> via a combined effect of winds, SST and thermocline DIC dynamics. Yasunaka et al., [2014] diagnosed decadal variability in the North Pacific DIC data (with neural network based pCO<sub>2</sub> modelling of Nakaoka et al.,

[2013]). McKinley et al., [2006] also examined decadal variability in the North Pacific using multi-model outputs and deduced the ensemble mean variability. Tjiputra et al., [2014] studied long term trends and future projections of global surface pCO<sub>2</sub> as simulated in five state-of-the-art earth system models.

### **1b. Remaining issues in our understanding of the equatorial Pacific carbon cycle variability on a variety of timescales**

From the previous studies discussed above, we have a clear understanding about the mechanisms of seasonal to interannual variability of the equatorial Pacific CO<sub>2</sub> fluxes and pCO<sub>2</sub> and also some insights into their decadal variability. However, our understanding of spatio-temporal evolution of these processes are still lacking [e.g., Wang et al. 2006b, Christian et al. 2008]. The longitudinal variation in the seasonal evolution of interannual variability of the carbon cycle in the equatorial Pacific has not been studied in detail despite the zonal contrast being the most fundamental aspect of ENSO dynamics. For example, the east-west evolution of air-sea CO<sub>2</sub> flux and pCO<sub>2</sub> variability during ENSO years are not clearly understood. Although this has been analysed for specific El Niño years (1994-95 and 1997-98) from observations [Feely et al., 1999, Sutton et al., 2014], a detailed account of processes over multiple interannual events (from last 50 years or longer) and their mechanisms are still to be elucidated.

On the other hand, the canonical ENSO is not the only process determining the interannual variability of the equatorial Pacific. During a canonical El Niño, the warming pattern is focused on the eastern equatorial Pacific even though the evolution of the warming was predominantly from east to west prior to the 1982-83 El Niño and from the dateline to the east for the subsequent El Niños till 1998 [Rasmusson and Carpenter 1982, Wang and An 2001]. This canonical or Eastern Pacific El Niño is typically captured in the first mode of the EOF of SST anomalies. However, recent studies have reported on different types of El Niños based on their surface expressions. They are referred to with various names in the literature such as El-Niño-Modoki or dateline El Niño, central Pacific El Niño (CP-El Niño), and Warm Pool ENSO [Yeh et al., 2009, Ashok et al., 2007, Larkin and Harrison, 2005, Kug et al., 2009]. El Niño-Modoki or the Central Pacific El Niño is characterised by a pattern of

central Pacific warming and two patches of cooling in the eastern and western equatorial Pacific [Ashok et al., 2007]. The debate about whether these are two distinct modes or different surface expressions of the same phenomenon continues [Takahashi et al. 2011, Johnson 2013] but some aspects of ENSO evolution may remain common across ENSO regimes [Ramesh and Murtugudde 2013]. The impact of the similarities and the differences of subsurface processes and surface expressions on the carbon cycle need further investigation.

In the wake of these findings, recent studies have focused on the chlorophyll-a variability in the equatorial Pacific and its relation to various types of ENSO [Turk et al., 2011, Radenac et al., 2012, Lee et al., 2014]. Biological changes during canonical El Niños are explained on the basis of strong and coherent variations in thermocline depth, wind-driven upwelling, nutrient supply and light, but changes associated with the El Niño-Modoki are more subtle and complex [Messie and Chavez, 2013]. However, the variability of pCO<sub>2</sub> and air-sea CO<sub>2</sub> fluxes related to these various types of ENSO over a multi-decadal period are yet to be fully analysed.

Regarding the mutli-decadal variability of carbon cycle in the equatorial Pacific, Feely et al., [2006] reveal a typical nature of the variability in that even with a steady increase of equatorial Pacific pCO<sub>2</sub> after the 1980s, the CO<sub>2</sub> outgassing is not increasing steadily in this region. This property is attributed to the overwhelming forcing of atmospheric CO<sub>2</sub> by anthropogenic emissions [Keeling et al., 2009]. On the other hand, the multi-decadal trends due to oceanic circulation changes [McPhaden and Zhang, 2004] may have the capacity either to offset or to accelerate the CO<sub>2</sub> emissions from the equatorial Pacific from epoch to epoch. Therefore our motivation to identify such internal variability in the equatorial Pacific carbon cycle is well-grounded, especially for assessing the role of oceans in the future as a sink of atmospheric CO<sub>2</sub> [Le Quere et al., 2013] and for deducing its feedback to global climate change. Moreover, the recent emergence of certain types of El Niño and their persistence in a warming climate [Collins et al., 2010] may have severe implication for oceanic emissions of CO<sub>2</sub> and global carbon budget.

Identifying the key unknowns in our understanding of the equatorial Pacific carbon cycle variability, we pose the following questions; (a) What are the spatio-temporal evolutions of CO<sub>2</sub> fluxes and pCO<sub>2</sub> in the equatorial Pacific during the dominant interannual mode, i.e., canonical ENSO? (b) How relevant are the spatial patterns of various El Niño types in terms of their impact on the CO<sub>2</sub> flux and pCO<sub>2</sub>? (c) What is the multi-decadal variability of the carbon cycle and what is its role in the long term variability of CO<sub>2</sub> sources of this region? and, (d) Are the multi-decadal changes (if they are detectable) robust and do they have any oceanic connection to the multi-decadal Pacific climate variability? There are no direct or readily available answers to the above questions from data or from models to the best of our knowledge. Therefore, in this study, we attempt to answer them based on a number of numerical experiments with a biogeochemical model.

The usual strategies of analysing the seasonal and interannual variability of the carbon cycle in the equatorial Pacific are by, (a) the direct analysis of observational or model time-series, (b) employing some statistical techniques such as empirical orthogonal functions (EOFs), (c) decomposing the total pCO<sub>2</sub> variability into dynamic, thermodynamic and biogeochemical components [McKinley et al., 2004, Le Quere et al., 2000, Wang et al. 2006b], (d) diagnosis using Taylor series expansions and linear regression analysis [Doney et al., 2009] and (e) multivariate analysis [Sabine et al., 2008]. Here we propose a different method of analysis based on EOFs carried out on a time-time matrix of anomalies unlike the conventional EOFs which are performed on a space-time domain. We demonstrate that through this method one can look at the spatial and temporal variability of seasonal evolution of a variable during dominant interannual events in a more instructive way.

The rest of the paper is framed as follows. Section 2 introduces the model and method of analyses used. Section 3 & 4 details the model validation with available observations and comparisons with other model results followed by the presentation of major results. Section 5 offers a discussion of results, followed by a summary in Section 6. Model uncertainties are given as Supplementary material.

## 2. Model and Analysis Methods

All the analyses made in this study are from a single model simulated with various configurations. The model employed here is an offline biogeochemical model as detailed in Valsala and Maksyutov, [2010] but with minor modifications as mentioned below.

### 2a. Physical model

The physical model used here is the Ocean Tracer Transport Model (OTTM) of Valsala et al., [2008]. The physical model is driven in an ‘offline mode’ by supplying the re-analysis data for ocean physical variables as inputs. The physical part of the model calculates the evolution of any passive tracer in the ocean by solving an advection-diffusion-source-sink equation explicitly on a spherical co-ordinate geometry. The surface seasonal vertical mixing is solved implicitly by matrix inversions. The model incorporates a self-operating diagnostic vertical mixing scheme based on the K-Profile-Parameterization [Large et al., 1994], isopycnal diffusion [Redi, 1982] and ‘bolus advections’ due to un-resolved eddies [Gent and McWilliams, 1992]. The necessary physical inputs for the model are temperature, salinity, ocean currents, surface heat, fresh water and river fluxes.

In this study, we used the offline data taken from GFDL’s coupled ocean-atmosphere re-analysis for the period from 1961 to 2005 [Chang et al., 2013, referred to as ECDv3.1 hereafter]. The assimilation system in ECDv3.1 consists of an Ensemble Filter applied to GFDL’s second generation fully coupled climate model [CM2.1; Delworth et al. 2006]. The ocean component of the coupled data assimilation (CDA) is the Modular Ocean Model version 4 [MOM4; Griffies et al. 2004] configured with 50 vertical levels (22 levels of 10-m thickness each in the top 220 m). The data were available at monthly resolutions for the 1961-2005 period (linearly interpolated to the model time step of 6 hrs) and for the global domain with approximately  $1^{\circ} \times 1^{\circ}$  resolution but telescopes down to meridional resolution of  $0.4^{\circ}$  around the equator. The poles are moved over land to avoid singularities. OTTM was run in the native grid of the offline input data with tri-polar grids.

The reanalysis products used here are the ‘best’ estimates from an assimilation system. The physical fields capture seasonal to decadal variability quite well [see Chang et al., 2013 for details]. For example, the Niño 3.4 index of SST anomalies reproduces the amplitude and variability of El Niño faithfully to the observations (see Figure 1; correlation of 0.96, significant at 99%). Figure 2 shows that El Niño-Modoki is also represented well. Because the physical fields employed are already bias corrected, the model uncertainties in terms of seasonal, interannual and interdecadal dynamics should be minimal. This gives us confidence in the reliability of the deduced carbon cycle variability from our study. As the results here show, the improved physics also leads to novel insights into the carbon cycle processes at seasonal-to-interannual and longer timescales.

## 2b. Biogeochemical Model

The chemical component of the biogeochemical model consists of a single tracer (DIC) as detailed in Valsala and Maksyutov [2010].  $p\text{CO}_2$  is treated as being in near equilibrium with the atmosphere at the sea surface via air-sea gas exchange. Within the ocean, DIC consists of carbonate and bicarbonate ( $\text{CO}_3^{2-}$ ,  $\text{HCO}_3^-$ ) ions and dissolved gaseous  $\text{CO}_2$ , although they are transported as a single tracer (DIC). This approach corresponds to the solubility pump model described in Ocean Carbon Cycle Inter Comparison Project-II (OCMIP-II; Orr et al., 1999).

Air-sea exchange of  $\text{CO}_2$  depends on piston velocity  $K_w$  and the difference in  $p\text{CO}_2$  between the surface ocean and the ambient atmosphere above. Alkalinity (taken as total alkalinity, TA) is not transported but is estimated from the reanalysis salinity inputs with a constant conversion factor of  $2310 \mu\text{eq kg}^{-1}$  as,  $\text{TA} = 2310 \cdot S/S_g$ , in which  $S$  is the local surface salinity and  $S_g$  is the annual mean surface salinity, averaged globally. This relation is taken from the OCMIP-II protocol [Orr et al., 1999].

The air-sea flux is formulated as  $\Phi_{\text{GASEX}} = K_w \kappa (p\text{CO}_{2\text{AIR}} - p\text{CO}_{2\text{OCEAN}})$ . The Henry’s constant,  $\kappa$ , and model  $p\text{CO}_2$  are calculated using the routines provided in OCMIP-II [Orr et al., 1999]. The term  $K_w$  is the piston velocity at which gaseous  $\text{CO}_2$  enters or leaves

the surface according to wind speed and CO<sub>2</sub> solubility, as formulated in Wanninkhof [1992]. We stick to this formulation although several variations to this were suggested by Sweeney et al., [2007] and Feely et al., [2004]. We use a gas exchange proportionality constant of 0.31 taken from OCMIP-II [Orr et al., 1999] when calculating  $K_w$ . Surface wind speed for the calculation of  $K_w$  is the sum of 10-day averages of 6-hourly squared wind speed ( $u^2_{10}$ ) and 6-hourly wind speed variance ( $\sigma^2 u_{10}$ ). Here,  $u_{10}$  indicates wind speed at 10 m height and is taken from NCEP/NCAR re-analysis-1 [Kalnay et al., 1996]. An index for polar ice-caps is used to partially mask the air-sea gas exchange during sea-ice conditions. This is achieved by compiling a spatial map of the ice index with values varying between 0.2 and 1.0.

The freshening of DIC by rain (P) and concentration by evaporation (E) is accounted for by E-P virtual fluxes of CO<sub>2</sub>. In addition, the riverine input of fresh water is also accounted for as a linear term in the DIC equation to induce dilution proportionally to the net rate of river input. However, the riverine input of DIC is not considered because a reliable global data set is not available.

The biological model employed here is similar to that of Valsala and Maksyutov [2010], which is originally derived from McKinley et al. [2004] with minor modifications as described below. In the present model, net export production in the euphotic zone (0-140m) is calculated from model derived phosphate (P) and light availability (I). In the previous version of the model in Valsala and Maksyutov [2010], the climatological phosphate from world ocean atlas (WOA) was directly used but has been modified with the model transported phosphate in this version of the model. Below 2000m, the model phosphate is restored to observed climatology with a relaxation time-scale of one year.

In the biological model, a mask term ‘ $\alpha$ ’ is used to represent other controlling factors of export rates that are not represented by the simple phosphate and light-limitation model [see Valsala and Maksyutov, 2010 for details]. In this case, the value of ‘ $\alpha$ ’ should be consistent with the model’s circulation and climatological nutrient fields. The global ocean is divided into 14 regions and the value of ‘ $\alpha$ ’ in each region is defined based on the assumption that a given model flow field will produce an annual mean phosphate distribution consistent

with climatological observations [McKinley et al., 2004]. The oceanic regions for ‘ $\alpha$ ’ are taken from McKinley et al. [2004], whereas the individual regional values of ‘ $\alpha$ ’ are tuned for the circulation used in this study. The half-saturation values for phosphate ( $P_0$ ) and light ( $I_0$ ) are set to  $0.01 \mu\text{mol kg}^{-1}$  and  $30 \text{ Wm}^{-2}$ , respectively.

Fluxes of sinking particles  $F(z)$  and remineralization below the euphotic zone depth are calculated as in OCMIP-II routines, with export profile following a power law represented in the form  $(z/100)^{-a}$  where  $z$  is depth in meters. The value of power ‘ $a$ ’ is fixed in most of the regions to 0.9 as per the recommendations of Yamanaka and Tajika [1997] and varies from 0.4 to 0.9 in tropical areas together with ‘ $a$ ’ values to constrain the model phosphate profiles close to the climatology.

## 2c. Observational datasets

Sea surface temperature data from Hadley Centre Global Sea Ice and Sea Surface Temperature [HadISST V1; Rayner et al. 2003] available at  $1^{\circ}\text{x}1^{\circ}$  is used for the EOF analysis and also for computing the Niño 3.4 and El Niño-Modoki indices [Ashok et al., 2007]. Global climatological air-sea  $\text{CO}_2$  flux data (adjusted to the Year-2000 winds and SST), available at a  $5^{\circ}\text{x}4^{\circ}$  resolution from the synthesis of Takahashi et al., [2009] is used for the model-data inter-comparisons.

## 2d. Model Experiments

Five model simulations are presented here, termed S1 through S5.

S1: The initial conditions for DIC for this run are taken from Global Ocean Data Analysis Project (GLODAP) observations [Key et al., 2004] and those for phosphate are taken from WOA-2005 [Garcia et al., 2006]. The physical variables for driving the model are specified as monthly climatologies constructed for years 1961-2010. The atmospheric  $\text{CO}_2$  is fixed at 315 ppm corresponding to the 1961 value. The model is run for 45 years by looping through the climatological physical forcing every year. This ‘spin-up’ run gives the upper

ocean (0-1000m) model DIC, phosphate, surface ocean pCO<sub>2</sub> and air-sea CO<sub>2</sub> fluxes close to equilibrium with minimum drift during the last 10 years of the simulation.

S2: The model is restarted from the last 10-year averages of DIC and phosphate of S1, and run through 1961 to 2005 using monthly varying physical fields. The atmospheric pCO<sub>2</sub> is fixed at 315 ppm. This simulation is done to infer how the physical circulation variability imprints on the carbon cycle for the past 45 years for a given atmospheric mole fraction of CO<sub>2</sub>.

S3: This is same as S2, but with observed changes in the atmospheric pCO<sub>2</sub> from 1961 to 2005 [Keeling et al., 2009]. This run simulates the contemporary fluxes of air-sea CO<sub>2</sub> including both natural and anthropogenic components [Wanninkhof et al., 2013]. The difference between S3 and S2 gives the anthropogenic accumulation of carbon in the ocean solely due to the build-up of atmospheric CO<sub>2</sub>.

S4: This is same as S3, but the monthly mean climatological winds are used in the air-sea CO<sub>2</sub> flux calculations (those are used in S1). This experiment is performed to quantify the impact of interannually varying wind speeds on air-sea CO<sub>2</sub> fluxes by subtracting S4 from S3.

S5: This is same as S3, but with monthly climatological physical fields (same as those used in S1). This experiment allows us to assess the impact of changes in ocean dynamics on air-sea CO<sub>2</sub> fluxes by subtracting S5 from S3.

All the runs are carried out for a 45 year period. The interannual runs (S2 to S5) are from 1961 to 2005.

## 2e. Analysis methodology

Traditionally, the EOF analysis in a spatio-temporal domain is employed to find the dominant spatial structures and the associated time series [McKinley et al., 2004]. However, such analyses bring out the dominant modes of variability encapsulating the entire domain of analysis under one common phenomenon. Here we introduce a new way of calculating EOFs which is capable of capturing the seasonal evolutions of dominant interannual mode of CO<sub>2</sub> fluxes and pCO<sub>2</sub> at individual longitudes in the equatorial Pacific irrespective of the mechanism that controls their variability. In constructing the time-time matrix, we have the freedom to resolve dominant seasonal evolution at each grid point in the equatorial Pacific and ascribe their relation to various types of El Niño.

The matrix for our EOF analysis is constructed as follows. As a first step, the CO<sub>2</sub> flux anomalies (linearly de-trended and de-seasonalized) are averaged over 5°N-10°S in the equatorial Pacific. Then we construct a matrix of anomalies with months along the X-axis and years along the Y-axis for each point in the equatorial Pacific. For example, 45 years of monthly anomalies at 180°E in equatorial Pacific (averaged over 5°N-10°S) are represented as a matrix of size 45x12, in which the first column is composed of anomalies of all Januaries from 1961 to 2005, the second column is composed of anomalies of all Februaries from 1961 to 2005, and so on. Since the seasonal cycle of any dominant event in the equatorial Pacific extends beyond the calendar year (i.e., January-December), we padded the 1961 to 1962 monthly anomalies in the first row (i.e., from January-1961 through December-1962) and the 1962 to 1963 values in the second row and so on. This facilitates the analysis of the seasonal evolution of ENSO. Therefore the total size of the matrix in our case is 44x24, where 44 is the total number of years (45 minus one). The Eigen values of this matrix are found and only the first mode of EOF is presented here.

We repeat the process for all the longitudinal points from 150°E to 90°W (at 1° resolutions) in the equatorial Pacific. In this way, the first mode is capable of representing the seasonal evolution of the dominant interannual event at a given longitude in the equatorial Pacific irrespective of which climate mode controls that variability. The principle component

of the first mode comprises of 44 yearly values for individual longitudes. Both EOF-1 and PC-1 are presented as a Hovmuller-diagram for the ease of interpretation.

In order to find which climate mode dominates the CO<sub>2</sub> flux and pCO<sub>2</sub> variability at each location, we correlate the PC-1 of each location separately with the Niño 3.4 and El Niño-Modoki indices (EMI). The interpretations are done this way: if the correlation of PC-1 with canonical ENSO index peaks at any longitudinal point, then EOF-1 shows the seasonal evolution of CO<sub>2</sub> flux anomalies during canonical ENSO at that location. This is possible because at each longitude the EOF is found independently of its neighbourhood and thereby the PCs are intimately related to a particular interannual mode which can be inferred by correlating the respective climate index with the PC. Likewise, if the correlation of PC-1 and El Niño-Modoki index peaks at any longitudinal point then EOF-1 is interpreted as driven by the Modoki at that longitude.

### 3. Results

The physical model capability in simulating the passive tracers was done extensively by the analysis of Chlorofluorocarbon (CFC) simulation in several of the previous studies [Valsala, et al., 2008; 2010] and will not be repeated here. Instead, here we present the mean and interannual variability of the carbon cycle simulated by this model and their comparison with observational based estimates and with other model results. The physical fields used in the model and their validation with observations for the canonical and central Pacific El Niños are also presented in Section 2a.

#### 3a. Mean and variability of model CO<sub>2</sub> fluxes

S1 produces an annual and global mean CO<sub>2</sub> sink of 0.5 PgC yr<sup>-1</sup>, for an atmospheric pCO<sub>2</sub> of 315 ppm, a value corresponding to the early 1960s. A majority of this CO<sub>2</sub> sink is due to the river water input and the resulting DIC dilution specified in the model, which is examined in a repeated S1 simulation with river water flux in the DIC equation switched off. The global sink of CO<sub>2</sub> is reduced to near zero in this case.

S2 produces a global mean sink of  $0.33 \pm 0.41$  PgC yr $^{-1}$  for 1961 to 2005 with the RMS of the global interannual anomalies shown as the uncertainty. This captures the effect of dynamics on net variability of CO<sub>2</sub> fluxes for the prescribed atmospheric pCO<sub>2</sub> (that of early 1960s).

S3 estimates a global net sink of  $1.95 \pm 0.32$  PgC yr $^{-1}$  in the model calculated for the period of 1990 to 2005. This value can be compared with the contemporary CO<sub>2</sub> sink as estimated by Wanninkhof et al., [2013] which is  $1.18 \pm 0.4$  PgC yr $^{-1}$  corrected to the winds and SST for year 2000, but without accounting for the riverine DIC inputs. In our model, S3 was repeated by switching off the river water contribution to the DIC dilution, which leads to a global reduction in oceanic uptake of  $0.52 \pm 0.04$  PgC yr $^{-1}$  (from 1975 to 2005) yielding a net global sink of  $1.43$  PgC yr $^{-1}$  which is closer to the estimate of Wanninkhof et al., [2013]. An average global oceanic sink during 2000 is estimated to be close to  $2.0$  PgC yr $^{-1}$  by the Global Carbon Project [GCP; Le Quere et al., 2013] as well as the global riverine input corrected estimates of Regional Carbon Cycle Assessment Processes [RECCAP,  $2.0 \pm 0.6$  PgC yr $^{-1}$ , Wanninkhof et al., 2013]. Therefore our model estimates the net sink that is consistent with other models and observational estimates.

The annual mean pattern of CO<sub>2</sub> flux from S3 calculated over a period of 1990 to 2005 compares well with that of Takahashi et al., [2009] (Figure 3). The global patterns of tropical sources and the sinks over the subtropics, Southern Ocean, North Pacific and North Atlantic are reasonably simulated in the model. The tropical Pacific source is slightly overestimated with a mean of  $0.89 \pm 0.13$  PgC yr $^{-1}$  (for 1990 to 2005), which is nearly double the corresponding estimates from RECCAP ( $0.44 \pm 0.14$  PgC yr $^{-1}$ ; Ishii et al. [2014]) but close to other model estimates [McKinley et al., 2004, Le Quere et al., 2000]. A detailed comparison of our model estimates with RECCAP is given in Table 1.

Global integral of air-sea CO<sub>2</sub> fluxes over 1961-2005 in S3 is a net sink of  $\sim 0.5$  PgC yr $^{-1}$  during the early 1960s, and increases to  $\sim 2.5$  PgC yr $^{-1}$  quite linearly until 1982 with

considerable interannual variability (Figure 4a). However, a dramatic reduction in the global CO<sub>2</sub> sink is noticeable after the 1982 El Niño despite the growth rate of atmospheric CO<sub>2</sub> concentration [Keeling et al., 2009]. This is quite interesting in the context of multi-decadal variability. S3 show that from 1982 to 1995 (during which, notably, 1983-84, 1984-85 and 1988-89 were La Niña years) there was a steady decrease in global CO<sub>2</sub> sink and from 1995 onwards the global sink strengthened slightly. The corresponding trend in the model pCO<sub>2</sub> from 1982 to 1995 (discussed in Figure 15) is consistent with observational estimates of Feely et al., [2006]. Such changes in global trends of sink anomalies are attributed to global circulation changes [Le Quere et al., 2010, Séférian et al., 2013].

Previous modelling studies have demonstrated that the interannual variability of the global air-to-sea CO<sub>2</sub> flux is largely determined by the corresponding tropical Pacific variability. Unlike the previous studies which placed the tropical Pacific contribution to be ~70% [Le Quere et al., 2000, McKinley et al., 2004, Obata and Kitamura 2003], our study finds it to be only ~40% (Figure 4b). Largest anomalies (i.e., a reduced CO<sub>2</sub> source in the tropical Pacific) occur during 1982-83 and 1997-98, which are 20<sup>th</sup> century's two strongest El Niño events [McPhaden et al., 1999]. In S3, the global sink anomaly grows as large as 0.6 PgC yr<sup>-1</sup> during these events. These are comparable with those reported in previous modelling studies, atmospheric inversions and observations [Ishii et al., 2014, McKinley et al., 2005, Gurney et al., 2004, Feely et al., 2006, Chavez et al., 1999]. The global CO<sub>2</sub> flux anomalies correspond well to that of the tropical Pacific.

The tropical Pacific alone contributes to an anomalous reduction in CO<sub>2</sub> source by ~0.5 PgC yr<sup>-1</sup> (Figure 4b). The correlation between the global and tropical pacific CO<sub>2</sub> flux anomalies are 0.59 in our model, consistent with previous modelling studies, reaffirming model capability in simulating the carbon cycle variability. It should be noted that this is not surprising since the global reach of the tropical Pacific at low-frequencies is well known due to its massive heat source in the western Pacific warm pool and is conjectured to be important even at millennial timescales (Cane and Evans 2000). The entire trade wind system responds to ENSO and PDO and can be expected to be manifest in global air-sea CO<sub>2</sub> fluxes.

Before proceeding to the detailed analysis, we provide a comparison of seasonal cycle of CO<sub>2</sub> fluxes with that derived from the Takahashi et al., [2009] dataset, along two sections of the equatorial Pacific. The western equatorial Pacific (150°E-160°W, 5°N-10°S) and the eastern Pacific (160°W-90°W, 5°N-10°S) in S3 display a comparable seasonal cycle to that estimated from the measured pCO<sub>2</sub>. The seasonal cycle of western Pacific CO<sub>2</sub> fluxes is somewhat larger in magnitude in the model (Figure 5a). The seasonal minimum source in the observations occurs around June whereas the model simulates it during April-May. The seasonal maximum is seen only during October in the observations, while it occurs during September-October in the model. Eastern Pacific CO<sub>2</sub> fluxes in the model show a better seasonal comparison with the observations although the annual mean is almost double in the model (Figure 5b). Both the model and the observations show a seasonal minimum source during March-April and maximum during August. Figure 5c and 5d show the interannual CO<sub>2</sub> flux anomaly evolution in S3 from these two regions. The western equatorial Pacific shows a weakening of the source whereas it strengthens in the eastern equatorial Pacific. A 10 year-smoothing of the fluxes shows slight trends of CO<sub>2</sub> sources in these two regions but is not investigated further here.

We compare the global and tropical ocean CO<sub>2</sub> flux anomalies between our model and Le Quere et al., [2010] in Figure 6. Le Quere et al. [2010] employed an intermediate complexity biogeochemistry model in a global configuration with NCEP/NCAR winds and heat fluxes. A comparison of CO<sub>2</sub> flux anomalies between S3 and Le Quere et al. [2010] shows that the global anomalies (with the trend) of these two models are highly correlated (correlation coefficient of 0.81). The corresponding correlations of de-trended anomalies are 0.45 (both significant at 95% significance level). The magnitudes of anomalies are within a range of 0.9 to -1.8 PgC yr<sup>-1</sup>. The 30°S-30°N belt of the ocean also yields a reasonable agreement between these two models ( $r=0.57$  with the trend and  $r=0.33$  without the trend; both significant at 95% significance level). Despite the differences in the complexities of these two models, an excellent agreement in interannual anomalies of CO<sub>2</sub> fluxes indicates that the model results presented here are robust.

We have thus verified the fidelity of the model in resolving seasonal and interannual variability with respect to observations and other models. As a summary of these model

validations, we conclude that: (a) the physical variables used to drive the model taken from re-analysis data are the ‘best’ estimates of the ocean state, (b) global mean air-sea CO<sub>2</sub> fluxes simulated are in good agreement with the observations, (c) global and tropical Pacific CO<sub>2</sub> flux anomaly variabilities compare well with similar modelling efforts. However, we point out that the amplitudes of seasonal cycles in the equatorial Pacific are somewhat overestimated in our model but they should not have any significant influence on our subsequent analysis and the overall conclusions of the study.

### 3b. Seasonal Evolution of CO<sub>2</sub> fluxes and pCO<sub>2</sub> during different types of El Niños

For the canonical El Niños, during the pre-1976 era, the SST anomalies in the equatorial Pacific evolve as a warm anomaly in Niño-1 region (east coast) in the month of February-March of the El Niño year (i.e., Year:0) and progress westward through Niño-2 and 3.4 regions and decay in March-April of the following year (i.e., Year:+1) [Rasmussen and Carpenter, 1982]. In contrast, during the post-1976 era the corresponding anomalies appear around the dateline and evolve eastward [McPhaden and Zhang 1999, Wang and An 2002]. In order to confirm that our EOF methodology resolves the seasonal evolution of SST during ENSO events in the equatorial Pacific, we constructed the EOFs using our method (see Section 2e) with the SST anomalies themselves. The results are presented in Figure 7a (thick contours) for EOFs computed over 1961 to 2005. EOF-1 clearly captures the seasonal progression of SST anomalies as a composite during an ENSO event, i.e., that the SST anomalies evolve during February-March of Year:0 and terminate during April of Year:+1 and begin to cool thereafter. For comparison, EOF-1 of SST is overlaid as a black line in each panel a of Figures 9 to 13.

All the EOF patterns presented here have meaningful units and the PCs are normalized with the respective standard deviations. The EOF of CO<sub>2</sub> flux anomalies (colour shades in Figure 7a, units are in moles m<sup>-2</sup> yr<sup>-1</sup>) shows that the anomalies have a peak signal between 160°W to 120°W during June of Year:0 to January of Year:+1. The El Niño induces this type of variability as indicated by the significant correlation between PC-1 (Figure 7b) and the Niño 3.4 Index between these longitudes (Figure 7c). Figure 7c shows the PC1 - El Niño correlation as a thick-blue line and PC1 - El Niño-Modoki correlation as a thick-cyan

line (left axis) with significant correlations indicated by thick-black straight lines. The variance explained by EOF-1 at each longitude is displayed as a thick-black line (right axis). Positive values indicate a source and the multiplication of EOF-1 with PC-1 has the sign of interannual variability. PC-1 during 1982-83 and 1997-98 is negative. This indicates a negative CO<sub>2</sub> flux anomaly indicating a weaker CO<sub>2</sub> source or near-neutral condition stretching almost from 150°E to 90°W. The PC shows a propagating nature from central Pacific to the east (Figure 7b). The maximum amplitude of anomaly during 1982-83 is about 1.8 moles m<sup>-2</sup> yr<sup>-1</sup>. The 1997-98 El Niño however resulted in a weaker reduction in CO<sub>2</sub> source than the 1982-83 event in the model, which we later attribute to the phases of the multi-decadal variability in the model.

A peculiar nature of PC-1 in this EOF approach is that it correlates with the appropriate climate anomalies distinctly at individual longitudinal locations. For example the longitudinal band over which the PC-1 significantly correlates with canonical El Niño index has insignificant correlations with El Niño-Modoki and vice versa. Thus the EOF method here illuminates the natural mode of variability at each longitude independent of its neighbouring points, and this aids the main aim of this study, viz., to show how the spatio-temporal variability in the equatorial Pacific carbon cycle is established and what the underlying mechanisms are.

Generally, the CO<sub>2</sub> flux anomalies in the equatorial Pacific (170°W-90°W) co-evolve with the canonical El Niño. The distinct peak of CO<sub>2</sub> flux anomalies at the far eastern longitudes (i.e., between 110°W and 90°W), however, appear to be unrelated to the canonical El Niño as seen from the weak correlation between PC-1 of this region and the Niño3.4 index. Interestingly the correlation with the El Niño-Modoki is positive with significant peaks in this region, indicating that an enhanced CO<sub>2</sub> source is associated with the Modoki. Moreover, between 150°E-170°E in the far west, the dominant source anomalies are also positively correlated more with the Modoki. Thus it appears that, while the central-east Pacific (between 150°W-110°W) is the most favoured region for the canonical El Niño influence, the seasonal evolution over the eastern and western equatorial Pacific is mostly associated with El Niño-Modoki. In addition, the variance explained by EOF-1 decreases from 70% in the east to 25% in the west. Thus the amplitude of interannual variability of CO<sub>2</sub>

fluxes is minimal to the west of the dateline. Note that the traditional EOFs do not allow us to extract the spatial variability of the variance whereas our methodology quantifies the relative zonal dominance of the different types of El Niños.

In order to illustrate the detailed seasonal evolution of CO<sub>2</sub> flux anomalies, we average the EOF-1 pattern in Figure 7a over 150°W-110°W and present it as a line plot from Year:0 to +1 (Figure 8a) with negative values corresponding to a weakened CO<sub>2</sub> source. The corresponding SST evolution is also shown (both PC-1 are shown in Fig. 8b). Within this region, the CO<sub>2</sub> flux anomalies co-evolve with SST-anomalies during an El Niño. Note that the signs of the EOF and PC of SST anomalies are reversed for easy comparison. In order to extract the nature of CO<sub>2</sub> evolution during any particular El Niño year, one has to multiply the PC-1 (red-bars) with the EOF-1 shown in Figure 8a.

A close examination indicates that the model suffers latency in the CO<sub>2</sub> source revival to the normal conditions after an El Niño. There is a secondary peak with weakened CO<sub>2</sub> source during July-August-September of Year:+1 related to El Niño. The observational estimates by Feely et al., [2006] however did not reveal any such latency. The latency is also visible in Figure 8b, in which the PC-1 tends to persist even after the El Niño. This tendency is especially noticeable after the 1980s. Notably, Rödenbeck et al., [2014] reported that the eastern Pacific CO<sub>2</sub> flux interannual variability is delayed by 6 to 8 months with respect to the El Niño peak (as estimated from 1993-2011 CO<sub>2</sub> fluxes using a pCO<sub>2</sub> observation-driven mixed layer model). Whether this is a model artefact or something that was not resolved in Feely et al's, [2006] empirical estimate needs further investigation.

The corresponding EOFs of pCO<sub>2</sub> anomalies illustrate a slightly different pattern of seasonal evolutions in the equatorial Pacific (Figure 9). Such de-coupling of pCO<sub>2</sub> and air-sea CO<sub>2</sub> flux variability is understandable in that the wind induced interannual variability in the CO<sub>2</sub> fluxes has spatial and temporal dependencies and thus can induce a non-linearity in the CO<sub>2</sub> flux-pCO<sub>2</sub> relationship. The roles of SST and solubility pumps are other possible reasons to induce non-linearity in the pCO<sub>2</sub>-CO<sub>2</sub> flux relations. EOF-1 shows generally a single sign of anomalies of pCO<sub>2</sub> over the entire stretch of equatorial Pacific during El Niño years.

However, the correlation between PC-1 and El Niño index peaks only between longitude bands of  $140^{\circ}\text{W}$ - $130^{\circ}\text{W}$ . The largest anomalies are noted during 1982-83 and 1997-98 El Niño as inferred from the PC-1 amplitudes. Unlike  $\text{CO}_2$  fluxes, the  $\text{pCO}_2$  anomaly does not show any significant east-to-west propagation in PC-1 (Figure 9b).

The  $\text{pCO}_2$  has a distinct response to El Niño-Modoki especially in the western Pacific (to the west of  $150^{\circ}\text{W}$ ). The correlation of PC-1 and El Niño is weaker between  $150^{\circ}\text{E}$ - $150^{\circ}\text{W}$ , whereas the correlation with the Modoki is higher there. Not surprisingly,  $\text{pCO}_2$  displays strong variability in response to El Niño and its different types, while the  $\text{CO}_2$  fluxes are mostly dominated by the canonical El Niño alone. This indicates the role of winds in inducing a non-linear nature in the  $\text{CO}_2$  flux- $\text{pCO}_2$  relations.

### 3c. Effect of interannual winds on the variability $\text{CO}_2$ flux and $\text{pCO}_2$ .

In order to understand the individual role of winds and ocean dynamics on the interannual variability of  $\text{CO}_2$  fluxes and  $\text{pCO}_2$  and their spatio-temporal characteristics, we examine the S4 and S5 outputs (see method for details). The difference between S3 and S4 separates the effects of interannual winds on  $\text{CO}_2$  flux and  $\text{pCO}_2$  variability. EOFs are calculated on the detrended differences of  $\text{CO}_2$  fluxes and  $\text{pCO}_2$  from S3 and S4, respectively.

The effects of ENSO related interannual winds on  $\text{CO}_2$  fluxes are confined mostly between  $170^{\circ}\text{W}$ - $120^{\circ}\text{W}$  (Figure 10). Between these longitudes, the PC-1 correlates positively with the Niño 3.4 index, i.e., the  $\text{CO}_2$  source weakens anomalously in these longitude bands during a canonical El Niño because of weaker winds. The magnitude of the wind effect on reduction in  $\text{CO}_2$  sources during El Niño is around  $0.5 \text{ moles m}^{-2} \text{ yr}^{-1}$ . The anomaly starts to build up during April of Year:0 and continues up to January of Year:+1.

A peculiar property of wind effects revealed here is that to the west of  $170^{\circ}\text{W}$  up to  $170^{\circ}\text{E}$ , the PC-1 correlation with Niño 3.4 index drops abruptly while that of the El Niño-

Modoki index goes up. In this longitudinal band, El Niño-Modoki tends to induce a weakening of CO<sub>2</sub> source by the corresponding wind anomalies (correlation is negative) at a moderate amplitude of 0.4 moles m<sup>-2</sup> yr<sup>-1</sup>. These subtle zonal variabilities are important and can be effectively be extracted by our methodology.

The wind effect on interannual pCO<sub>2</sub> is generally an increase of about 5 μatm on average (Figure 11). The peak increase is centred between 170°W-120°W where the canonical El Niño is in control. The maximum pCO<sub>2</sub> change is about 12 μatm. Between 170°E and 170°W, El Niño-Modoki causes an increase in pCO<sub>2</sub> of about 5 μatm. The increase in pCO<sub>2</sub> due to the interannual wind effects is mainly by the reduction in CO<sub>2</sub> sources as seen in Figure 10.

### 3d. Effect of interannual ocean dynamics on the variability of CO<sub>2</sub> flux and pCO<sub>2</sub>

Similarly, we examined the effect of ocean dynamics (i.e., the effects of circulation, SST and all related variables) on CO<sub>2</sub> flux and pCO<sub>2</sub> anomalies in the equatorial Pacific and their spatio-temporal characteristics and relation to various types of interannual variability. This was done by examining the difference between S3 and S5. EOFs were computed for the detrended differences between S3 and S5 and results are depicted in Figures 12 and 13.

The effects of dynamics show that CO<sub>2</sub> anomalies are generated during a canonical El Niño, especially between 160°W-120°W. A reduction in CO<sub>2</sub> source by the ocean dynamics alone is up to 0.6 moles m<sup>-2</sup> yr<sup>-1</sup>. Interestingly the net dynamical effect between 170°W-140°W is a negative anomaly (i.e., weakened CO<sub>2</sub> source) during Year:0 and up to the March of Year:+1, and a sudden revival as a positive anomaly (i.e., a strengthened CO<sub>2</sub> source) thereafter. This property, however, is not seen between 140°W-100°W, indicating a strong zonal variability in the dynamical control. To the west of 170°W, the El Niño-Modoki-induced dynamics has more influence than El Niño-induced dynamics. The correlation between PC-1 and El Niño-Modoki increases in this zone, while the effect of El Niño diminishes. The dynamic effects on pCO<sub>2</sub> are explored in Figure 13. The El Niño dynamics control the pCO<sub>2</sub> variability between 160°E-120°W while the Modoki- dynamics dominate in

two longitudinal bands between  $140^{\circ}\text{W}$ - $90^{\circ}\text{W}$  and between  $150^{\circ}\text{W}$ - $150^{\circ}\text{E}$ . The amplitude of the anomaly is about  $6 \mu\text{atm}$ .

Figure 14 summarizes the zonal contrasts of the spatio-temporal influences of El Niño and El Niño-Modoki on CO<sub>2</sub> flux and pCO<sub>2</sub> anomalies in the equatorial Pacific as inferred from detailed analyses above. In the region between  $160^{\circ}\text{W}$ - $110^{\circ}\text{W}$ ,  $10^{\circ}\text{S}$ - $5^{\circ}\text{N}$ , El Niño dominates the variability of CO<sub>2</sub> flux and pCO<sub>2</sub> (mean and RMS of anomalies from 1961 to 2005 is  $0.43 \pm 0.12 \text{ PgC yr}^{-1}$ ). However, the western (EMI\_1,  $160^{\circ}\text{E}$ - $160^{\circ}\text{W}$ ) and far eastern (EMI\_2,  $110^{\circ}\text{W}$ - $90^{\circ}\text{W}$ ) equatorial Pacific CO<sub>2</sub> flux and pCO<sub>2</sub> variability are predominantly influenced by El Niño-Modoki ( $0.3 \pm 0.06$  and  $0.11 \pm 0.04 \text{ PgC yr}^{-1}$  for EMI\_1 and EMI\_2, respectively). Thus, out of a total CO<sub>2</sub> emission of  $0.83 \pm 0.14 \text{ PgC yr}^{-1}$  from the equatorial Pacific ( $160^{\circ}\text{E}$ - $90^{\circ}\text{W}$ ,  $10^{\circ}\text{S}$ - $5^{\circ}\text{N}$ ), one half of the entire stretch (i.e., the central and east Pacific) is influenced by El Niño with a flux magnitude of  $\sim 0.4 \text{ PgC yr}^{-1}$  and the remaining half is dominated by the other type of El Niño. The individual effects of winds and ocean dynamics on total carbon cycle variability are intricately intertwined from region to region in the equatorial Pacific. However, the net effects are still discernibly distinct between El Niño and El Niño-Modoki.

#### 4. Multi-decadal variability

The global anomalies of CO<sub>2</sub> sinks (Figure 4a) show a steady increase in CO<sub>2</sub> uptake in response to the atmospheric growth rate from 1961 to 1982, whereas after the 1982-83 El Niño event, there is an apparent shift in the global sink anomaly, with a reduced uptake rate until 2000. A slight increase is seen in the sink during the 1997-98 El Niño, and the sink continues to increase thereafter. Figure 4b reveals that most of the global sink anomalies are explained solely by the variability in the tropical Pacific. The increased pCO<sub>2</sub> in the equatorial Pacific after the 1980s was also noted in Feely et al., [2006] from observations. Therefore the model result is consistent with what the observations suggest. Our analysis suggests that such abrupt climate shifts in CO<sub>2</sub> sink anomalies were due to multi-decadal variability in the equatorial Pacific.

In order to elucidate the multi-decadal variability, we smoothed the CO<sub>2</sub> flux anomaly with a 10-year running mean from 1961 to 2005 (Figure 15). The dominant powers of 10-year smoothed data of pCO<sub>2</sub> anomalies are confined mostly to the equatorial Pacific. The eastern tropical Indian and Atlantic Oceans also display some decadal signals. The clear anchoring of the strongest CO<sub>2</sub> flux and pCO<sub>2</sub> multi-decadal variability in the equatorial Pacific is rather intriguing. There are no other parts in the global ocean where such variability is found in our model simulations, at least above a variance of 10  $\mu\text{atm}^2$ .

The area integrated CO<sub>2</sub> flux and pCO<sub>2</sub> anomalies in the equatorial Pacific ( $130^0\text{E}$ - $290^0\text{E}$ ,  $5^0\text{N}$ - $5^0\text{S}$ ) smoothed by a 10-year running mean clearly show a multi-decadal signal as seen in Figure 15b and c. The anomalies show a weakening of CO<sub>2</sub> source (seen as negative anomalies) from 1961 to 1981 and a strengthening thereafter until 1991. After 1991 the source weakens again. We examined similar area averages in S5 (thin full line) and S4 (dash line) outputs. S5 reproduces the decadal variability but S4 has no such signal, highlighting that the variability in ocean dynamics is the major reason for multi-decadal variability in the equatorial Pacific pCO<sub>2</sub> and CO<sub>2</sub> fluxes [Guilderson and Schrag, 1998, Wang and An, 2002].

In both Figures 15b and c, we overlay the corresponding smoothed SST anomalies averaged over the same region. There appears to be a tentative and inverse relationship between SST and CO<sub>2</sub> flux/pCO<sub>2</sub> variability. The reduction in CO<sub>2</sub> sources during the 1980s and the corresponding warmer SSTs can be attributed to an anomalous ocean convergence and a reduction in DIC divergence, pCO<sub>2</sub> and in CO<sub>2</sub> source. However, there is a phase shift between the SST anomalies and the CO<sub>2</sub> flux and pCO<sub>2</sub> anomalies, respectively, on multi-decadal timescale. The wavelet spectrum of 10-year running mean smoothed pCO<sub>2</sub> data of Figure 15c shows a dominant signal with an apparent 15-18 year cycle (Figure 16), which is explored further below. The stippled areas show a significant variability at 90% confidence level in the chi-square test and significant multi-decadal signal is clearly seen during 1970-2005, which has not been reported before, to the best of our knowledge.

The decadal variance larger than 10  $\mu\text{atm}^2$  in pCO<sub>2</sub> is clearly situated in the equatorial Pacific. However, this variability may have a much broader structure in the interior of the

ocean. The oceanic tropical convergent cells (a shallow meridional overturning cell in the equatorial Pacific connecting tropical and subtropical oceans) exhibit multi-decadal variability in-phase with PDO [McPhaden and Zhang, 2004]. Therefore, we examined the cause of the decadal signal in the surface ocean pCO<sub>2</sub> and its connection to the ocean interior by analysing the model DIC anomalies. By following the variability of meridional overturning cell in the tropical-subtropical Pacific as described in McPhaden and Zhang [2004], we averaged the DIC anomalies of S3 from 160°E-90°W and carried out a conventional EOF analysis in spatio-temporal domain from 40°N-30°S and from surface to 1500 meters.

EOF-1 of DIC anomalies in the meridional and vertical sections show an increase in DIC anomalies in the equatorial Pacific, invading down to a depth of 1200 m and stretching to the northern Pacific along the permanent-thermocline pathways anchored around 600 m depth (Figure 17a, units are in  $\mu\text{mole kg}^{-1}$ ). In the southern hemisphere, however, a counter part of this cell is not apparent in the DIC anomalies. While comparing with the modes of variability over the Pacific, we find the maximum correlation of first three PCs with the PDO, Modoki and Niño 3.4 indices, respectively. The PC-1 reproduces a clear multi-decadal signal centred in the early 1980s. PC-1 is correlated significantly with the PDO index smoothed with a 10-year running mean. The correlation is  $\sim -0.5$ . There is, however, a phase shift observed between the PC-1 and the smoothed PDO index (PDO lags PC-1). EOF-1 explains 21% of the variance.

EOF-2 is rather surface trapped with complex small-scale patterns of DIC anomalies with a meridional extent covering the entire tropics (Figure 17b). PC-2 shows an interesting decadal signal which is correlated with the corresponding scale variability in El Niño-Modoki index ( $r = -0.54$ ) which is smoothed with a 4-year running mean. This mode explains 13% of the DIC variance.

EOF-3 shows a clear equatorially trapped signal with a penetration down to 600 m at the equator (Figure 17c). The meridional extent of this mode is quite constrained between

$10^{\circ}\text{S}$ - $10^{\circ}\text{N}$ . PC-3 correlates well with the El Niño index suggesting that the DIC variability of this type (12% of total variance) is related to El Niño.

EOF-1 is clearly able to trace and link the multi-decadal signal revealed in the equatorial Pacific pCO<sub>2</sub> to the northern Pacific via interior oceanic pathways. This result should be reiterated in-light of the conclusions of Ishii et al., [2009] that the western Pacific warm pool DIC observations show similar decadal signals which they accurately attributed to the variability in the geostrophic convergence into the equator from northern and southern subtropics [also see McPhaden and Zhang, 2004]. Moreover, Sabine et al., [2008] affirmed that such decadal trends occur in the north Pacific subsurface DIC based on observations. Our model results are thus consistent with the physical and biogeochemical variability reported before by other independent studies.

McPhaden and Zhang [2004] pointed out that the tropical convergence cell displays a decadal variability, most of which is related to the PDO and the anomalous advection of the mean temperatures. Our analysis indicates, not surprisingly, that a similar variability exists in the carbon cycle of the tropical Pacific and this variability is also modulated by the PDO and thus operates through the ocean circulation associated with the PDO. The impacts of these PDO modulations are to induce multi-decadal secular trends in sources of CO<sub>2</sub> fluxes and pCO<sub>2</sub> in the equatorial Pacific.

## 5. Discussion

The study demonstrates a novel approach to computing EOFs on a time-time domain of anomalies at each longitude separately. With this new methodology we are able to discern the spatio-temporal structures of equatorial Pacific carbon cycle variability and are able to associate them with the two types of ENSO. Moreover, we are able to identify the variance of the interannual anomalies at each location in the equatorial region and are able to evaluate the amplitude of a particular variability of CO<sub>2</sub> flux and pCO<sub>2</sub> at any location in the equatorial Pacific at interannual time-scales.

The conventional space-time EOFs of equatorial Pacific variables usually yield El Niño induced variability as EOF-1 and the Modoki as EOF-2 [Ashok et al., 2007]. However, our methodology illustrates the CO<sub>2</sub> flux and pCO<sub>2</sub> variability related to the canonical El Niño and Modoki in just a single EOF, which clearly requires an explanation. When we do time-time EOF, we are extracting the dominant time-scale at each location and the EOF-1 extracts a dominant El Niño-Modoki time-scale in the west and the canonical El Niño in the east. The complementarily varying correlations of PCs with indices for different types of El Niño provide a clear clue for understanding the dominant physical mode of variability and mechanisms of CO<sub>2</sub> flux and pCO<sub>2</sub> at each zonal location. The zonally contrasted variability and the responsible processes identified here nicely complement previous studies and provide additional insights into the zonal specificity of the canonical El Niño and the central Pacific El Niño or the Modoki [see also Le Quere et al., 2000, McKinley et al., 2004].

A peculiar nature of the PCs retrieved this way is worth discussing. To be more specific, Figure 10b and 12b appear somewhat discontinuous at around 165°W and 135°W. Such discontinuity indicates a temporal ‘lead or lag’ in the correlation between PCs of two neighbouring locations in the longitudinal direction. If such a particular lead or lag persists over a region then it is an indicator of the direction of propagation of anomalies during an interannual event (i.e., either from west to east or vice-versa). We computed lead-lag correlations of PCs between two neighbouring points of longitudes over the entire domain from 150°E-90°W (figure not shown). In the case of Figure 10b and 12b, the correlations indicate that within 165°W and 140°W the anomalies responsible for the CO<sub>2</sub> flux variability propagate from east-to-west whereas outside of this zone, the anomalies propagate in the opposite direction. Therefore, the EOFs computed in this manner are also instructive of the direction of propagations of interannual events, a technique worth exploring with other data sets too.

The evolution of canonical El Niños during pre-1976 is considerably different from that of the post-1976 era both in the seasonality and in the locations of the warm and cold anomalies during the seasonal progression of the El Niño [Trenberth et al, 2001; McPhaden and Zhang 2009; Ren and Jin 2011]. In a separate calculation we divided the time domain into pre-1976 and post-1976 periods and repeated the EOF analysis for these two epochs separately (figure not shown). The EOF-1 loading of seasonal evolutions of CO<sub>2</sub> fluxes and pCO<sub>2</sub> show slight differences between these two epochs, whereas the PCs remain nearly

identical to the one deduced from the analysis of the total period. One noticeable feature is that the CO<sub>2</sub> source anomalies, especially in the eastern most part of the equatorial Pacific, is more pronounced in the post-1976 era than in the pre-1976, indicative of the role of El Niño-Modoki rather than the canonical El Niño in causing such anomalies. The CO<sub>2</sub> flux variability of the far eastern part of the equatorial Pacific, particularly as a CO<sub>2</sub> source, is more closely linked to El Niño-Modoki than El Niño (see Figure 7). The emergence of more frequent El Niño-Modokis in the post-1976 period [Ashok et al., 2007] may be generating such source anomalies in the CO<sub>2</sub> responses in the far eastern equatorial Pacific.

The role of multi-decadal variability in generating the secular decadal trends of air-sea CO<sub>2</sub> fluxes in the equatorial Pacific is worth mentioning. Feely et al., [2006] show that even with a steady increase of equatorial Pacific pCO<sub>2</sub> after the 1980s, the CO<sub>2</sub> outgassing is not increasing steadily because the atmospheric growth rate of CO<sub>2</sub> is much faster than the oceanic build-up in this region. Therefore, multi-decadal trends due to oceanic circulation changes have the capacity to either offset or to accelerate the CO<sub>2</sub> emissions from the equatorial Pacific. Identifying such internal variability is a crucial step in assessing the role of the ocean in the future as a sink of atmospheric CO<sub>2</sub> [Le Quere et al., 2013]. The effect of El Niño and its various flavours on CO<sub>2</sub> fluxes in the equatorial Pacific are spatially and temporally locked to certain locations in the equatorial Pacific. Canonical El Niño tends to reduce the source of CO<sub>2</sub> from the equatorial Pacific whereas the corresponding reduction in the CO<sub>2</sub> sources by the El Niño-Modoki is smaller in magnitude. Therefore, the emergence of a certain type of El Niño and its persistence in a warming climate [Collins et al., 2010, Power et al., 2013] has severe implication in the oceanic emissions of CO<sub>2</sub> and global carbon budget. The role of these factors in the net CO<sub>2</sub> transfer between the ocean and atmosphere is a topic worth examining. Further studies are warranted in this direction since the ENSO response to global warming remains highly model dependent.

The anchoring of multi-decadal variability of air-sea CO<sub>2</sub> fluxes and pCO<sub>2</sub> in the equatorial Pacific is rather intriguing. The variance of multi-decadal signal in pCO<sub>2</sub> greater than 10  $\mu\text{atm}^2$  is hardly visible in the global ocean except in the equatorial Pacific. Such large variances could be a model artefact and need to be validated. The multi-decadal variability in the biological production in various oceanic regions is noted in past studies [Mantua et al., 1997] even though the impact of such subtle decadal changes on the net pCO<sub>2</sub> variance is less clear in our model. We did examine the multi-decadal variance of amplitude below 10  $\mu\text{atm}^2$

in our model. Regions with foot-prints of low amplitude decadal variability are indeed present (also see Valsala et al., 2012). The four-polar structure of pCO<sub>2</sub> and air-sea CO<sub>2</sub> flux variability in the north Pacific in-phase with the PDO (Valsala et al., 2012) are visible in the present model as well albeit as low amplitude signals of pCO<sub>2</sub>.

The DIC variability is able to track the multi-decadal signal of equatorial Pacific pCO<sub>2</sub> and air-sea CO<sub>2</sub> fluxes to the north Pacific and connect to the time-scales of PDO via the variability in tropical convergence [McPhaden and Zhang, 2004, Ishii et al., 2009, Sabine et al., 2008]. Interestingly, similar decadal variability in the tropical - subtropical exchange of thermocline and deep waters is also detected in other ocean re-analysis data set [Valsala et al., 2011 and their Figure 6, top panel]. Further studies with more comprehensive biogeochemistry models are required to completely assess the equatorial Pacific carbon cycle variability and their relation to PDO.

## 6. Summary

Using an offline model of the global ocean biogeochemistry driven by re-analysis physical fields, we examine in detail the simulated spatio-temporal evolution of interannual-to-decadal variability of air-sea CO<sub>2</sub> fluxes and pCO<sub>2</sub> in the equatorial Pacific for 45 years from 1961 to 2005. A new methodology of EOF constructed over a time-time domain of anomalies over the equatorial Pacific (averaged over 5°N-10°S) is employed. This methodology extracts the seasonal evolution of the dominant mode of variability of CO<sub>2</sub> fluxes and pCO<sub>2</sub> at each longitudinal point in the equatorial Pacific.

In the region between 160°W-110°W in the equatorial Pacific (averaged over 5°N-10°S), El Niño controls the dominant variability of CO<sub>2</sub> fluxes. In the western (160°E-160°W) and far eastern (110°W-90°W) equatorial Pacific, CO<sub>2</sub> flux variability is dominantly influenced by El Niño-Modoki. On the other hand, the interannual variability of pCO<sub>2</sub> is correlated with El Niño mostly to the east of 140°W and with El Niño-Modoki to the west of 140°W. The de-coupling of CO<sub>2</sub> flux and pCO<sub>2</sub> variability at various locations in the equatorial Pacific are attributable to the differences in the combined and individual effects of ocean dynamics and winds. The effects of the two types of El Niño on CO<sub>2</sub> fluxes in the equatorial Pacific are

spatially and temporally locked to certain locations in the equatorial Pacific but this may depend on the impact of global warming on El Niño itself.

A multi-decadal variability in the equatorial Pacific CO<sub>2</sub> fluxes and pCO<sub>2</sub> emerges with positive phases in the 1960s and 2000s and a negative phase in 1980s. The oceanic DIC anomalies are able to trace this decadal signal to the northern Pacific via thermocline pathways, presumably related to the phase shifts of PDO and subsequent variability in the tropical - subtropical Pacific convergence cell variability. The study comprehensively assembles the various aspects of spatial and temporal variability of the equatorial Pacific carbon cycle over a variety of time scales from seasonal to multi-decadal. Identifying such internal variability is a crucial step in assessing the role of the ocean in the future as a sink of atmospheric CO<sub>2</sub> [Le Quere et al., 2013].

Considering the fidelity of ocean re-analysis used to run the model and the comparisons offered between the observations and other modelling studies, the results identified here are robust. Our novel EOF approach captures the local seasonal evolution of the anomalies of pCO<sub>2</sub> and CO<sub>2</sub> fluxes at each longitude, which should facilitate future model and data analyses for solubility and biological pumps, to understand the rich spectrum of timescales in the equatorial Pacific (or any other regions of the global ocean).

## 7. Acknowledgement

The re-analysis data were obtained from <http://www.gfdl.noaa.gov/ocean-data-assimilation>. HadISST v1 is obtained from <http://www.metoffice.gov.uk/hadobs/hadisst/>. NCEP/NCAR Re-1 data downloaded from <http://www.esrl.noaa.gov/psd/data/gridded/data.ncep.reanalysis.html>. Area integrated CO<sub>2</sub> fluxes from Le Quere et al., [2010] shown in Figure 6 are digitized from their Figure 5 using GetData Graph Digitizer (<http://getdata-graph-digitizer.com>). Ms. Preethi Bhaskar, IITM is gratefully acknowledged for the assistance in the wavelet analysis. Model development and computations were carried out at High Performance Computing Facility of IITM. The model outputs of this study and software can be freely provided for research purposes upon request sent to the corresponding author. This works was funded by Ministry of Earth Sciences (MoES), Govt. of India through its various programs in IITM.

Accepted

## 8. References

- Ashok K, S. K. Behera, S. Rao, et al. [2007]: El Niño Modoki and its possible teleconnection. *J Geophys Res* 112:C11007, doi:10.1029/2006JC003798.
- Cane, M. A. and M. N. Evans, 2000: Climate variability - Do the tropics rule? *Science*, 290 (5494): 1107-1108
- Chang, Y.-S., S. Zhang, A. Rosati, T. Delworth, and W. F. Stern, [2013]: An assessment of oceanic variability for 1960-2010 from the GFDL ensemble coupled data assimilation, *Climate Dynamic*, Volume 40, Issue 3-4, pp 775-803, 10.1007/s00382-012-1412-2
- Chavez, F. P., P. G. Strutton, G. E. Friederich, R. A. Feely, G. Feldman, D. Foley, and M. J. McPhaden [1999]: Biological and chemical response of the equatorial Pacific Ocean to the 1997-1998 El Niño, *Science*, 286, 2126-2131.
- Christian, J. R., R. A. Feely, M. Ishii, R. Murtugudde, and X. Wang, [2008]: Testing an ocean carbon model with observed sea surface pCO<sub>2</sub> and DIC in the tropical Pacific. *J Geophys Res.*, 113, C07047, doi:10.1029/2007JC004428.
- Christian, J., M. Verschell, R. Murtugudde, A. Busalacchi, and C. McClain, [2001]: Biogeochemical modeling of the tropical Pacific Ocean I: Seasonal and interannual variability. *Deep Sea Res. II*, 49, 509-543, doi:10.1016/S0967-0645(01)00110-2
- Cosca, C. E., R. A. Feely, J. Boutin, J. Etcheto, and M. J. McPhaden [2003]: Seasonal and interannual CO<sub>2</sub> fluxes for the central and eastern equatorial Pacific Ocean as determined from fCO<sub>2</sub>-SST relationships, *J. Geophys. Res.*, 108(C8), 3278, doi: 10.1029/2000JC000677.
- Collins et al., [2010]: The impact of global warming on the tropical Pacific Ocean and El Niño, *Nature Geoscience*, 3, 391 – 397, doi:10.1038/ngeo868
- Delworth et al., [2006]: GFDL's CM2 Global Coupled Climate Models. Part I: Formulation and simulation characteristics. *J. Climate*, 19, 643–674. doi:<http://dx.doi.org/10.1175/JCLI3629.1>
- Doney, S. C., Ivan Lima, Richard A. Feely, David M. Glover, Keith Lindsay, Natalie Mahowald, J. Keith Moore, R. Wanninkhof [2009]: Mechanisms governing interannual variability in upper-ocean inorganic carbon system and air-sea CO<sub>2</sub> fluxes: Physical climate and atmospheric dust, *Deep Sea Research-II*, 56, 640-655, doi:10.1016/j.dsr2.2008.12.006
- Etcheto, J., J. Boutin, Y. Dandonneau, D. C. E. Bakker, R. A. Feely, R. D. Ling, P. D. Nightingale, N. Metzl, and R. Wanninkhof [1999]: (1999), Air-sea CO<sub>2</sub> flux variability in the equatorial Pacific Ocean near 100°W. *Tellus B*, 51: 734–747. doi: 10.1034/j.1600-0889.1999.t01-1-00013.x
- Fay, A. R., and G. A. McKinley, [2013]: Global trends in surface ocean pCO<sub>2</sub> from in situ data, *Global Biogeochem. Cycles*, 27, 541–557, doi:10.1002/gbc.20051.

Feely, R. A. R. Wanninkhof, C. E. Cosca, P. P. Murphy, M. F. Lamb, M. D. Steckley, [1995]: CO<sub>2</sub> distributions in the equatorial Pacific during the 1991–1992 ENSO event, Deep Sea Res., II, Volume 42, 365–386, doi:10.1016/0967-0645(95)00027-N

Feely, R. A., et al., [2002]: Seasonal and interannual variability of CO<sub>2</sub> in the equatorial Pacific, Deep Sea Res- II, 49(13-14), 2443-2469.

Feely, R. A., R. Wanninkhof, T. Takahashi, P. Tans [1999]: Influence of El Niño on the equatorial Pacific contribution to atmospheric CO<sub>2</sub> accumulation, Nature, 01/1999; 398(6728):597-601. DOI:10.1038/19273

Feely, R. A., R. Wanninkhof, W. McGillis, M.-E Carr. and C. E. Cosca [2004]: Effects of wind speed and gas exchange parameterizations on the air-sea CO<sub>2</sub> fluxes in the equatorial Pacific Ocean, Journal of Geophys. Res., Vol 109, C08S03, doi:10.1029/2003JC001896.

Feely, R. A., T. Takahashi, R. Wanninkhof, M. J. McPhaden, C. E. Cosca, S. C. Sutherland, and M.-E. Carr [2006]: Decadal variability of the air-sea CO<sub>2</sub> fluxes in the equatorial Pacific Ocean, J. Geophys. Res., 111, C08S90, doi:10.1029/2005JC003129

Feely, R.A., R. Wanninkhof, C. Goyet, D.E. Archer, and T. Takahashi [1997]: Variability of CO<sub>2</sub> distributions and sea-air fluxes in the central and eastern equatorial Pacific during the 1991–1994 El Niño, Deep-Sea Res. Pt. II, 44(9–10), doi: 10.1016/S0967-0645(97)00061-1, 1851–1867

Friedrichs, M, et al., [2009]: Assessing the uncertainties of model estimates of primary productivity in the tropical Pacific, Journal of Marine Systems, 76, 113-133, doi:10.1016/j.jmarsys.2008.05.010

Garcia, H. E., R. A. Locarnini, T. P. Boyer, and J. I. Antonov, [2006]: World Ocean Atlas 2005, Volume 4: Nutrients (phosphate, nitrate, silicate). S. Levitus, Ed. NOAA Atlas NESDIS 64, U.S. Government Printing Office, Washington, D.C., 396 pp.

Gent, P. R., and J. C. McWilliams, [1990]: Isopycnal mixing in ocean circulation models. J. Phys. Oceanogr., 20, 150–155.doi: [http://dx.doi.org/10.1175/1520-0485\(1990\)020<0150:IMIOCM>2.0.CO;2](http://dx.doi.org/10.1175/1520-0485(1990)020<0150:IMIOCM>2.0.CO;2)

Gierach, M. M., T. Lee, D. Turk, and M. J. McPaden [2012]: Biological response to the 1997-98 and 2009-10 El Nino events in the equatorial Pacific Ocean, Geophys. Res. Lett., 39, L10602, doi:10.1029/2012GL051103.

Griffies, S. M., M. J. Harrison, R. C. Pacanowski, and A. Rosati, [2004]: A Technical Guide to MOM4. GFDL Ocean Group Technical Report No. 5, Princeton, NJ: NOAA/Geophysical Fluid Dynamics Laboratory, 342 pp.

Gruber, M. Gloor, M., Fletcher, S. E. M., Doney, S. C., Dutkiewicz, S. and co-authors, [2009]: Oceanic sources, sinks and transport of atmospheric CO<sub>2</sub>. Global Biogeochem. Cycles 23, doi:10.1029/2008GB003349.

Gurney, K. R., Law, R. M., Denning, A. S., Rayner, P. J., Pak, B. and Transom-3-L2-modelers, [2004]: Transcom-3 inversion intercomparison: control results for the estimation of

seasonal carbon sources and sinks. Global Biogeochem. Cycles 18, doi:10.1029/2003GB002111.

Guilderson, T.P. and D.P. Schrag [1998]: Abrupt shift in subsurface temperatures in the tropical Pacific associated with changes in El Niño, Science 281, 240- 243, DOI: 10.1126/science.281.5374.240

Ishii, M., H. Y. Inoue, T. Midorikawa, S. Saito, T. Tokieda, D. Sasano, A. Nakadate, K. Nemoto, N. Metzl, C.S. Wong, R. A. Feely, Spatial variability and decadal trend of the oceanic CO<sub>2</sub> in the western equatorial Pacific warm/fresh water [2009]: Deep Sea Research Part II: Topical Studies in Oceanography, 56, 591-606, doi:10.1016/j.dsr2.2009.01.002

Ishii, M., R. A. Feely, K. B. Rodgers, G-H Park, R. Wanninkhof, D. Sasano, H. Sugimoto, C. E. Cosca, S. Nakaoka, M. Telszewski, Y. Nojiri, S. E. Fletcher, Y. Niwa, P. K. Patra, V. Valsala, H. Nakano, I. Lima, S. C. Doney, E. T. Buitenhuis, O. Aumont, [2014]: Air-sea CO<sub>2</sub> flux in the Pacific Ocean for the period 1990-2009, Biogeosciences 11 (3), 709-734

Jochum, M., S. Yeager, K. Lindsay, K. Moore, and R. Murtugudde, 2010: Quantification of the Feedback between Phytoplankton and ENSO in the Community Climate System Model. J. Climate, 23, 2916–2925, doi: <http://dx.doi.org/10.1175/2010JCLI3254.1>

Jones, C. D., M. Collins, P. M. Cox, S. A. Spall, [2001]: The Carbon Cycle Response to ENSO: A Coupled Climate–Carbon Cycle Model Study. J. Climate, 14, 4113–4129. doi: <http://dx.doi.org/10.1175/1520-0442>

Johnson, N. C., [2013]: How Many ENSO Flavors Can We Distinguish?. J. Climate, 26, 4816–4827. doi: <http://dx.doi.org/10.1175/JCLI-D-12-00649.1>

Kalnay, E., M. Kanamitsu, R. Kistler, W. Collins, D. Deaven, L. Gandin, M. Iredell, S. Saha, G. White, J. Woollen, Y. Zhu, A. Leetmaa, R. Reynolds, M. Chelliah, W. Ebisuzaki, W. Higgins, J. Janowiak, K. C. Mo, C. Ropelewski, J. Wang, Roy Jenne, and Dennis Joseph, 1996: The NCEP/NCAR 40-Year Reanalysis Project. Bull. Amer. Meteor. Soc., 77, 437–471. doi: [http://dx.doi.org/10.1175/1520-0477\(1996\)077<0437:TNYRP>2.0.CO;2](http://dx.doi.org/10.1175/1520-0477(1996)077<0437:TNYRP>2.0.CO;2)

Keeling, R.F., S.C. Piper, A.F. Bollenbacher and J.S. Walker. [2009]: Atmospheric CO<sub>2</sub> records from sites in the SIO air sampling network. In Trends: A Compendium of Data on Global Change. Carbon Dioxide Information Analysis Center, Oak Ridge National Laboratory, U.S. Department of Energy, Oak Ridge, Tenn., U.S.A. doi: 10.3334/CDIAC/atg.035

Key, R. M., Kozyr, A., Sabine, C. L., Lee, K., Wanninkhof, R. and co-authors. [2004]: A global ocean carbon climatology: results from Global Ocean Data Analysis Project (GLODAP). J. Geophys. Res. 18, doi:10.1029/2004GB002247.

Kug, J.-S., F.-F. Jin, and S.-I. An [2009]: Two types of El Niño events: Cold Tongue El Niño and Warm Pool El Niño, J. Clim., 22, 1499–1515, doi:10.1175/2008JCLI2624.1.

Landschützer, P., N. Gruber, D. C. E. Bakker, and U. Schuster (2014), Recent variability of the global ocean carbon sink, Global Biogeochem. Cycles, 28, doi:10.1002/2014GB004853.

Large, W. G., J. C. McWilliams, and S. C. Doney (1994), Oceanic vertical mixing: A review and a model with a nonlocal boundary layer parameterization, *Rev. Geophys.*, 32(4), 363–403, doi:10.1029/94RG01872.

Larkin N. K., and D. E. Harrison [2005]: On the definition of El Niño and associated seasonal average U.S. weather anomalies. *Geophys. Res. Lett.*, 32, L13705, doi:10.1029/2005GL022738.

Le Quere, C., Orr, J. C., Monfray, P., Aumont, O. and Madec, G. [2000]: Interannual variability of the oceanic sink of CO<sub>2</sub> from 1979 through 1997. *Global Biogeochem. Cycles* 14, 1247–1265.

Le Quere, C., et al., [2013], Global Carbon Budget 2013, *Earth System Science Data Discussion*. doi: 10.5194/essdd-6-689-2013.

Le Quéré, C., T. Takahashi, E. T. Buitenhuis, C. Rödenbeck, and S. C. Sutherland (2010), Impact of climate change and variability on the global oceanic sink of CO<sub>2</sub>, *Global Biogeochem. Cycles*, 24, GB4007, doi:10.1029/2009GB003599.

Lee, K.-W., S.-W. Yeh, J.-S. Kug, and J.-Y. Park [2014]: Ocean chlorophyll response to two types of El Niño events in an ocean-biogeochemical coupled model, *J. Geophys. Res. Oceans*, 119, 933–952, doi:10.1002/2013JC009050.

Li Y. and Y. Xu [2013]: Interannual variations of the air-sea carbon dioxide exchange in the different regions of the Pacific Ocean, *Acta Oceanologica Sinica*, 32, 3, 71-79, 10.1007/s13131-013-0291-7

Mantua, N.J. and S.R. Hare, Y. Zhang, J.M. Wallace, and R.C. Francis [1997]: A Pacific interdecadal climate oscillation with impacts on salmon production. *Bulletin of the American Meteorological Society*, 78, pp. 1069-1079.

McKinley, G. A., Follows, M. J. and Marshall, J. [2004]: Mechanism of air-sea CO<sub>2</sub> flux variability in the equatorial Pacific and North Atlantic. *Global Biogeochem. Cycles* 18, doi:10.1029/2003GB002179.

McKinley, G.A., T. Takahashi, E. Buitenhuis, F. Chai, J. R. Christian, S. C. Doney, M.-S. Jiang, C. Le Quere, I. Lima, K. Lindsay, J.K. Moore, R. Murtugudde, L. Shi, P. Wetzel [2006]: North Pacific carbon cycle response to climate variability on seasonal to decadal timescales. *J. Geophys. Res.*, 111, C07S06, doi:10.1029/2005JC003173.

McKinley, G.A., C. Rodenbeck, M. Gloor, S. Houweling and M. Heimann [2005]: Pacific dominance to global air-sea CO<sub>2</sub> flux variability: A novel atmospheric inversion agrees with ocean models. *Geophys. Res. Lett.*, 31, GL22308, doi: 10.1029/2004GL021069.

McPhaden, M. J., and X. Zhang [2009]: Asymmetry in zonal phase propagation of ENSO seasurface temperature anomalies, *Geophys. Res. Lett.*, 36, L13703, doi:10.1029/2009GL038774

McPhaden, M. J., and D. Zhang [2004]: Pacific Ocean Circulation rebounds, *Geophys. Res. Lett.*, 31, L18301, doi:10.1029/2004GL020727

Messie, M., and F. P. Chavez [2013]: Physical-biological synchrony in the global ocean associated with recent variability in the central and western equatorial Pacific, *J. Geophys. Res. Oceans*, 118, 3782–3794, doi:10.1002/jgrc.20278.

Murtugudde, R., J. Beauchamp, C. R. McClain, M. Lewis, and A. J. Busalacchi, 2002: Effects of Penetrative Radiation on the Upper Tropical Ocean Circulation. *J. Climate*, 15, 470–486. doi: [http://dx.doi.org/10.1175/1520-0442\(2002\)015<0470:EOPROT>2.0.CO;2](http://dx.doi.org/10.1175/1520-0442(2002)015<0470:EOPROT>2.0.CO;2)

Murtugudde, R. G., S. R. Signorini, J. R. Christian, A. J. Busalacchi, C. R. McClain, and J. Picaut (1999), Ocean color variability of the tropical Indo-Pacific basin observed by SeaWiFS during 1997–98, *J. Geophys. Res.*, 104, 18,351–18,366, doi:10.1029/1999JC900135.

Nakaoka, S., M. Telszewski, Y. Nojiri, S. Yasunaka, C. Miyazaki, H. Mukai, and N. Usui [2013]: Estimating temporal and spatial variation of sea surface pCO<sub>2</sub> in the North Pacific using a self-organizing map neural network technique, *Biogeosciences*, 10, 6093–6106, doi:10.5194/bg-10-6093-2013.

Orr, J. C., Najjar, R., Sabine, C. L. and Joos, F. [1999]: Abiotic-HOWTO. LSCE/CEA Saclay, Gif-sur-Yvette, France, 25 pp.

Obata, A. and Kitamura, Y. 2003. Interannual variability of the air-sea exchange of CO<sub>2</sub> from 1961 to 1998 simulated with a global ocean circulation-biogeochemistry model. *J. Geophys. Res.* 108, doi:10.1029/2001JC001088.

Park, G.-H., R. Wanninkhof, S. C. Doney, T. Takahashi, K. Lee, R. A. Feely,C. L. Sabine, J. Trinanes, I. D. Lima, [2010]: Variability of global net sea-air CO<sub>2</sub> fluxes over the last three decades using empirical relationships, *Tellus B*, 62, 352–368. doi: 10.1111/j.1600-0889.2010.00498.x

Patra, P. K., J.K. Moore, N. Mahowald, M. Uematsu, S.C. Doney and T. Nakazawa, [2007]: Exploring the sensitivity of basin-scale air-sea CO<sub>2</sub> fluxes to interannual to decadal variability in atmospheric dust deposition using ocean carbon models and atmospheric CO<sub>2</sub> inversions, *J. Geophys. Res. - Biogeochemistry*, 112, G02012, 2007

Patra, P. K., Maksyutov, S., Ishizawa, M., Nakazawa, T., Takahashi, T. and co-authors. [2005]: Interannual and decadal changes in the air-sea CO<sub>2</sub> flux from atmospheric CO<sub>2</sub> inverse modeling. *Global Biogeochem.Cycles* 19, doi:10.1029/2004GB002257.

Picaut, J., M. Ioualalen, T. Delcroix, F. Masia, R. Murtugudde, and J. Vialard, [2001]: Displacements of an Oceanic Zone of Convergence on the eastern edge of the Pacific warm pool: Consequences for ENSO and biogeochemical phenomena. *J. Geophys. Res.*, 106, 2363-2386.

J. Picaut, F. Masia, Y. du Penhoat [1997]: An Advective-Reflective Conceptual Model for the Oscillatory Nature of the ENSO. *Science*, 277, 663-666, DOI: 10.1126/science.277.5326.663

Power, S., F. Delage, C. Chung, G. Kociuba and K. Keay, [2013]: Robust twenty-first-century projections of ElNiño and related precipitation variability , *Nature*, Vol 502, doi:10.1038/nature12580

Radenac, M.-H., F. Léger, A. Singh, and T. Delcroix [2012]: Sea surface chlorophyll signature in the tropical Pacific during eastern and central Pacific ENSO events, *J. Geophys. Res.*, 117, C04007, doi:10.1029/2011JC007841.

Rasmusson M. E., and T. H. Carpenter, [1982]: Variations in Tropical Sea Surface Temperature and Surface Wind Fields Associated with the Southern Oscillation/El Niño. *Mon. Wea. Rev.*, 110, 354–384.doi: [http://dx.doi.org/10.1175/1520-0493\(1982\)110<0354:VITSST>2.0.CO;2](http://dx.doi.org/10.1175/1520-0493(1982)110<0354:VITSST>2.0.CO;2)

Ramesh, N., and R. Murtugudde, [2013]: All flavors of El Niño have Similar Sub surface Origins. *Nature Clim. Chang.*, 3, 42-46. doi:10.1038/nclimate1600.

Rayner, N.A., D.E. Parker, E.B. Horton, C.K. Folland, L.V. Alexander, D.P. Rowell, E.C. Kent, and A. Kaplan, [2003]: Global analyses of sea surface temperature, sea ice, and night marine air temperature since the late nineteenth century. *J. Geophys. Res.* 108(14), 2-1,DOI: 10.1029/2002JD002670.

Redi, M., [1982]: Oceanic isopycnal mixing by coordinate rotation. *J. Phys. Oceanogr.*, 12, 1154–1158.

Ren, H.-L., and F.-F. Jin [2011]: Niño indices for two types of ENSO, *Geophys. Res. Lett.*, 38, L04704, doi:10.1029/2010GL046031

Rödenbeck, C., Bakker, D. C. E., Metzl, N., Olsen, A., Sabine, C., Cassar, N., Reum, F., Keeling, R. F., and Heimann, M.: Interannual sea-air CO<sub>2</sub> flux variability from an observation-driven ocean mixed-layer scheme, [2014]: *Biogeosciences Discuss.*, 11, 3167-3207, doi:10.5194/bgd-11-3167-2014.

Sabine, C. L., R. A. Feely, F. J. Millero, A. G. Dickson, C. Langdon, S. Mecking, and D. Greeley (2008), Decadal changes in Pacific carbon, *J. Geophys. Res.*, 113, C07021, doi:10.1029/2007JC004577.

Sarma, V. V. S. S., A. Lenton, R. M. Law, N. Metzl, P. K. Patra, S. Doney, I. D. Lima, E. Dlugokencky, M. Ramonet, and V. Valsala, [2013]: Sea-air CO<sub>2</sub> fluxes in the Indian Ocean between 1990 and 2009, *Biogeosciences*, 10, 7035-7052, 2013

Séférian, R., Bopp, L., Swingedouw, D., and Servonnat, J.: Dynamical and biogeochemical control on the decadal variability of ocean carbon fluxes, [2013]: *Earth Syst. Dynam.*, 4, 109-127, doi:10.5194/esd-4-109-2013.

Sutton, A., R. Feely, C. L. Sabine et al., [2014]: Natural variability and anthropogenic change in equatorial Pacific surface ocean pCO<sub>2</sub> and pH, *Global Biogeochemical Cycles*, doi:10.1002/2013GB00469.

Schuster, U., G. A. McKinley, N. Bates, F. Chevallier, S. C. Doney, A. R. Fay, M. González-Dávila, N. Gruber, S. Jones, J. Krijnen, P. Landschützer, N. Lefèvre, M. Manizza, J. Mathis, N. Metzl, A. Olsen, A. F. Rios, C. Rödenbeck, J. M. Santana-Casiano, T. Takahashi, R. Wanninkhof, and A. J. Watson, [2013], An assessment of the Atlantic and Arctic sea-air CO<sub>2</sub> fluxes, 1990–2009, *Biogeosciences*, 10, 607-627, 2013

Sweeney, C., E. Gloor, A. R. Jacobson, R. M. Key, G. McKinley, J. L. Sarmiento and R. Wanninkhof [2007]: Constraining global air-sea gas exchange for CO<sub>2</sub> with recent bomb C-14 measurements. *Global Biogeochemical Cycles* 21 (2). DOI: 10.1029/2006GB002784

Takahashi T, Sutherland SC, Sweeney C, Poisson A, Metzl N, Tilbrook B, Bates N, Wanninkhof R, Feely RA, Sabine C, Olafsson J, Nojiri Y [2002]: Global sea-air CO<sub>2</sub> flux based on climatological surface ocean pCO<sub>2</sub> and seasonal biological and temperature effect. *Deep-Sea Res* 49:1601–1622

Takahashi, T., S. C. Sutherland, R. A. Feely, C. E. Cosca, [2003]:, Decadal Variation of the Surface Water PCO<sub>2</sub> in the Western and Central Equatorial Pacific, *Science* 31 October 2003: Vol. 302 no. 5646 pp. 852-856, DOI: 10.1126/science.1088570

Takahashi, T., Sutherland, S. C. Wanninkhof, R., Sweeney, C., Feely, R. A. and co-authors. [2009]: Climatological mean and decadal change in surface ocean pCO<sub>2</sub>, and net sea-air CO<sub>2</sub> flux over the global oceans. *Deep-Sea Res.* II 56, 554–577, doi:10.1016/j.dsr2.2008.12.009

Tans, P. P., I. Y. Fung, and T. Takahashi [1990]: Observational Constraints on the Global Atmospheric Co<sub>2</sub> Budget, *Science*, 247, 1431-1438, DOI: 10.1126/science.247.4949.1431

Tjiputra J. F., A. Olsen, L. Bopp, A. Lenton, B. PFEIL, T. ROY, J. Segschneider, I. Totterdell, and C. Heinze, [2014]: Long-term surface pCO<sub>2</sub> trends from observations and models, *Tellus-B*, 66, 23083, doi:10.3402/tellusb.v66.23083

Trenberth, K. E., D. P. Stepaniak, J. W. Hurrell and M. Fiorino [2001]: Indices of El Niño evolution, *J. Climate*, 14, 1697-1701.

Torrence C., and G. P. Compo, 1998: A Practical Guide to Wavelet Analysis. *Bull. Amer. Meteor. Soc.*, 79, 61–78.doi: [http://dx.doi.org/10.1175/1520-0477\(1998\)079<0061:APGTWA>2.0.CO;2](http://dx.doi.org/10.1175/1520-0477(1998)079<0061:APGTWA>2.0.CO;2)

Turk, D., C. S. Meinen, D. Antoine, M. J. McPhaden, and M. R. Lewis [2011]: Implications of changing El Niño patterns for biological dynamics in the equatorial Pacific Ocean, *Geophys. Res. Lett.*, 38, L23603, doi:10.1029/2011GL049674.

Valsala V., S. Maksyutov and R. Murtugudde, [2011]: Interannual to Interdecadal Variabilities of the Indonesian Throughflow Source Water Pathways in the Pacific Ocean, *J. Phys. Oceanography*, 41, 1921-1940.

Valsala V., H. M. Alsibai, M. Ikeda and S. Maksyutov, [2010]: Interannual variability of CFC-11 absorption by the ocean: an offline model study, *Climate Dynamics*, 36, 1435-1452, doi:10.1007/s00382-010-0784-4

Valsala V., Maksyutov, S., and Ikeda, M. [2008]: Design and validation of an offline Oceanic Tracer Transport Model for Carbon Cycle Study, *J. Climate*, 21, 2752–2769, 2008.

Valsala, V., Maksyutov, S., Telszewski, M., Nakaoka, S., Nojiri, Y., Ikeda, M., and Murtugudde, R.: Climate impacts on the structures of the North Pacific air-sea CO<sub>2</sub> flux variability, *Biogeosciences*, 9, 477-492, doi:10.5194/bg-9-477-2012, 2012.

Valsala V. and S. Maksyutov, [2010]: Simulation and assimilation of global ocean pCO<sub>2</sub> and air-sea CO<sub>2</sub> fluxes using ship observations of surface ocean pCO<sub>2</sub> in a simplified biogeochemical offline model. *Tellus B*, 62: 821–840. doi: 10.1111/j.1600-0889.2010.00495.x

Wanninkhof, R. 1992. Relationship between wind speed and gas exchange over the ocean. *J. Geophys. Res.* 97, 7373–738

Wanninkhof, R., G. -H. Park, T. Takahashi, C. Sweeney, R. Feely, Y. Nojiri, N. Gruber, S. C. Doney, G. A. McKinley, A. Lenton, C. Le Quéré, C. Heinze, J. Schwinger, H. Graven, and S. Khatiwala, [2013]: Global ocean carbon uptake: magnitude, variability and trends, *Biogeosciences*, 10, 1983–2000, 20132.

Wang, B., and S. An, [2002]: A mechanism for decadal changes of ENSO behaviour: Roles of background wind changes. *Climate Dynamics*, 18, 475–486, 10.1007/s00382-001-0189-5

Wang X. J., J. R. Christian, R. Murtugudde, A. J. Busalacchi, [2006]: Spatial and temporal variability of the surface water pCO(2) and air-sea CO<sub>2</sub> flux in the equatorial Pacific during 1980–2003: a basin-scale carbon cycle model. *J. Geophys. Res.*, 111, C07S04.

Wang, X., J. R. Christian, R. Murtugudde, and A. J. Busalacchi, [2005]: Ecosystem dynamics and export production in the central and eastern equatorial Pacific: A modeling study of impact of ENSO. *Geophys. Res. Lett.*, 32, L2608.

Wang, X., J. R. Christian, R. Murtugudde, and A. J. Busalacchi, [2006]: Spatial and temporal variability in new production in the equatorial Pacific during 1980–2003: physical and biogeochemical controls. *Deep Sea Res Part II*, 53, 677–697.

Yasunaka, S., Y. Nojiri, S.-i. Nakaoka, T. Ono, H. Mukai, and N. Usui [2014]: North Pacific dissolved inorganic carbon variations related to the Pacific Decadal Oscillation, *Geophys. Res. Lett.*, 41, 1005–1011, doi:10.1002/2013GL058987.

Yamanaka, Y., and E. Tajika (1997), Role of dissolved organic matter in the marine biogeochemical cycle: Studies using an ocean biogeochemical general circulation model, *Global Biogeochem. Cycles*, 11(4), 599–612, doi:10.1029/97GB02301.

Yeh S. W, J. S. Kug, B. Dewitte, M. Kowan, B. P. Kirtman and F. F. Jin [2009]: El Niño in a changing climate, *Nature*, 461, 511–514., doi:10.1038/nature08316

## Table captions

**Table 1:** Global and tropical Pacific ( $18^{\circ}\text{S}$ - $18^{\circ}\text{N}$ )  $\text{CO}_2$  fluxes from this study are compared with RECCAP estimates. All units are in  $\text{PgC yr}^{-1}$ .

## Figure captions

**Figure 1:** Normalized Niño 3.4 SST anomalies ( $170^{\circ}\text{W}$ - $120^{\circ}\text{W}$ ,  $5^{\circ}\text{N}$ - $5^{\circ}\text{S}$ ) from the ocean re-analysis data (full line) and that from the HadISST (boxes). Correlation between the two indices from 1961 to 2010 is 0.92. The high correspondence between two indices shows the fidelity of the ocean re-analysis.

**Figure 2:** Same as previous figure but for El Niño-Modoki (EMI) index. EMI index is calculated as in Ashok et al., [2007]. Correlation between the indices is 0.9 over the entire period from 1960 to 2010.

**Figure 3:** [a] 1990-2005 average of global ocean surface sea-to-air  $\text{CO}_2$  fluxes from the model. Global total sink during this period is  $1.95 \pm 0.32 \text{ PgC yr}^{-1}$ . [b] Sea-to-air  $\text{CO}_2$  fluxes from Takahashi et al., [2009] database. Units are in  $\text{moles m}^{-2} \text{ yr}^{-1}$ .

**Figure 4:** [a] Global integral of total sea-to-air  $\text{CO}_2$  fluxes from 1961 to 2005 estimated by the model. [b] The model de-trended and de-seasonalized global total sea-to-air  $\text{CO}_2$  flux anomalies (left axis) and corresponding tropical Pacific ( $160^{\circ}\text{E}$ - $280^{\circ}\text{E}$ ,  $15^{\circ}\text{N}$ - $15^{\circ}\text{S}$ ) flux anomalies (right axis). Tropical Pacific  $\text{CO}_2$  flux anomalies are significantly correlated with global anomalies ( $r = 0.59$ ) and explain ~40% global anomaly variance. The thick red line is the 12-month running mean of global  $\text{CO}_2$  flux anomalies.

**Figure 5:** [a, b] Seasonal cycle of sea-to-air  $\text{CO}_2$  fluxes from western and eastern equatorial Pacific shown as comparisons between model and Takahashi et al., [2009]. [c, d] Interannual  $\text{CO}_2$  flux anomalies from the model integrated over western and eastern Pacific equatorial. The black lines show the 10-year running mean. All units are in  $\text{PgC yr}^{-1}$ .

**Figure 6:** Comparison of [a] Global and [b]  $30^{\circ}\text{S}$ - $30^{\circ}\text{N}$  belt of ocean  $\text{CO}_2$  flux anomalies between our model and LeQuere et al., [2010]. Correlations are given. Anomalies shown here

are computed with respect to 1960–1981 climatological mean in order for the calculations to be consistent with Le Quere et al., [2010].

**Figure 7:** [a] Seasonal evolutions of the dominant mode of interannual variability (shown over two years; see text) of the equatorial Pacific CO<sub>2</sub> flux anomalies for each grid point from 160°E to 90°W (EOF-1, see section 2e for details). Colour shade represents CO<sub>2</sub> flux (moles m<sup>-2</sup> yr<sup>-1</sup>) and thick contour represents corresponding EOF-1 of sea surface temperature anomalies (SST; °C). [b] The principle components (PC-1; normalized) for each grid point from 160°E to 90°W. [c] Time-correlation between PC-1 and Niño 3.4 (blue) and El Niño-Modoki (cyan) from each grid point (left axis). The thick black line shows the variance explained by EOF-1 from each grid point (right axis).

**Figure 8:** [a] Seasonal evolutions of the dominant interannual sea-air CO<sub>2</sub> flux anomalies (left axis) and SST anomalies (right axis) from the central-to-east Pacific (spatially averaged between 150°W-110°W in Figure-2) and shown for Year:0 and +1. [b] The PC-1 of CO<sub>2</sub> flux anomalies (red bars and thick black line) and SST anomalies (blue bars). EOF-1 and PC-1 of SST have been reversed in sign for easy comparison. The correlation coefficient between PC-1 of CO<sub>2</sub> flux and SST is shown.

**Figure 9:** Same as Figure-7, but for pCO<sub>2</sub> anomalies (units are in μatm).

**Figure 10:** Same as Figure 7, but for CO<sub>2</sub> flux anomalies calculated as a difference between S3 and S4. The anomalies represent the effect of interannual variability in winds on CO<sub>2</sub> flux variability in the equatorial Pacific.

**Figure 11:** Same as Figure 10, but for pCO<sub>2</sub> anomalies.

**Figure 12:** Same as Figure 10, but for CO<sub>2</sub> flux anomalies calculated as a difference between S3 and S5. The anomalies represent the effect of interannual variability in ocean dynamics on CO<sub>2</sub> flux variability in the equatorial Pacific.

**Figure 13:** Same as Figure 12, but for pCO<sub>2</sub> anomalies.

**Figure 14:** Summary of spatial coverages of dominant interannual variability of CO<sub>2</sub> fluxes and pCO<sub>2</sub> in the equatorial Pacific segregated according to regionally dominant mechanisms identified from Figure 7 through 13. Canonical El Niño is the dominant mechanism of carbon cycle variability in the central-to-east equatorial Pacific, nearly overlapping with the Niño 3.4 region. In the western (EMI\_1, 160°E-160°W) and far eastern (EMI\_2, 110°W-90°W) equatorial Pacific El Niño-Modoki is the dominant mechanism. The dashed box shows a region of model uncertainty in pCO<sub>2</sub>-ENSO relations. The y-axis just indicates the variable names.

**Figure 15:** [a] Variance of 10-year smoothed pCO<sub>2</sub> anomalies calculated from 1961 to 2005 ( $\mu\text{atm}^2$ ). [b] Monthly CO<sub>2</sub> anomalies (de-trended and de-seasonalised) averaged over a box shown in (a) and smoothed by running mean over 10-years. Thick (thin) black line shows the CO<sub>2</sub> anomalies from S3 (S5) (see text for details). Thick dotted line shows the CO<sub>2</sub> anomalies from S4. The red lines show the SST anomalies averaged over the same box and smoothed by a 10-year running mean and scaled linearly to fit to the common y-axis. The solid (dashed) red lines show the SST anomalies from HadISST (GFDL re-analysis), respectively. [c] Same as (b) but for pCO<sub>2</sub> anomalies.

**Figure 16:** Wavelet power spectrum of the pCO<sub>2</sub> data shown in Figure 15c. The dots represent significance at 90% confidence level. Morlet wavelet is used and Fourier transform is performed [Torrence and Compo, 1998]. The wavelet power spectrum is defined as the absolute value squared of the wavelet transform and gives a measure of the time series variance at each scale (period) and at each time. Statistical significance is tested using Chi-square test.

**Figure 17:** EOF-1 to 3 of dissolved inorganic carbon (DIC) anomalies (de-trended and de-seasonalised) computed over a latitude-depth section and averaged zonally over the Pacific longitudes from 160°E-90°W. Left panels show the EOF loadings and the right panels show corresponding principle components. The red lines in the right panels show the PDO index (10-year running mean), El Niño-Modoki index (2-year running mean) and El Niño index (1-year running mean) from top to bottom, respectively. EOF-1 explains the dominant decadal signal with 23% variance. EOF-2 explains the second dominant signal with 13% variance, and EOF-3 shows the El Niño variability with 10% variance. EOF loadings are in  $\mu\text{mole kg}^{-1}$  and all PCs and climate indices are normalized.

**Table 1:** Global and tropical Pacific ( $18^{\circ}\text{S}$ - $18^{\circ}\text{N}$ ) CO<sub>2</sub> fluxes from this study are compared with RECCAP estimates. All units are in PgC yr<sup>-1</sup>.

Method	Global [Wanninkhof et al., 2013] <sup>a</sup>	Tropical Pacific Ishii et al., [2014] <sup>a</sup>		
	Median±Uncertainty	IAV	Median±Uncertainty	IAV <sup>c</sup>
pCO <sub>2</sub> data based estimate	-2.0 ± 0.60	0.20	0.51	0.27
OBGCM	-1.9 ± 0.30	0.16	0.41 ± 0.05	0.40
Atmospheric Inversion	-2.1 ± 0.30	0.40	0.53 ± 0.08	0.48
<b>This model<sup>b</sup></b>	<b>-1.95 ± 0.32<sup>e</sup></b>	<b>0.33<sup>d</sup></b>	<b>0.89 ± 0.13<sup>e</sup></b>	<b>0.13<sup>d</sup></b>

<sup>a</sup> Data from 1990-2009 are used. Median sea-air CO<sub>2</sub> fluxes are shown for the global and median±median absolute deviation of estimates from various models is shown for the tropical Pacific.

<sup>b</sup> Data from 1990-2005 are used.

<sup>c</sup> Interannual variability (IAV) is peak-to-peak difference of the annual mean flux.

<sup>d</sup> IAV is the standard deviation of the interannual CO<sub>2</sub> flux anomalies.

<sup>e</sup> Mean of S3 and uncertainty from interannual CO<sub>2</sub> flux anomalies from S2 are shown.

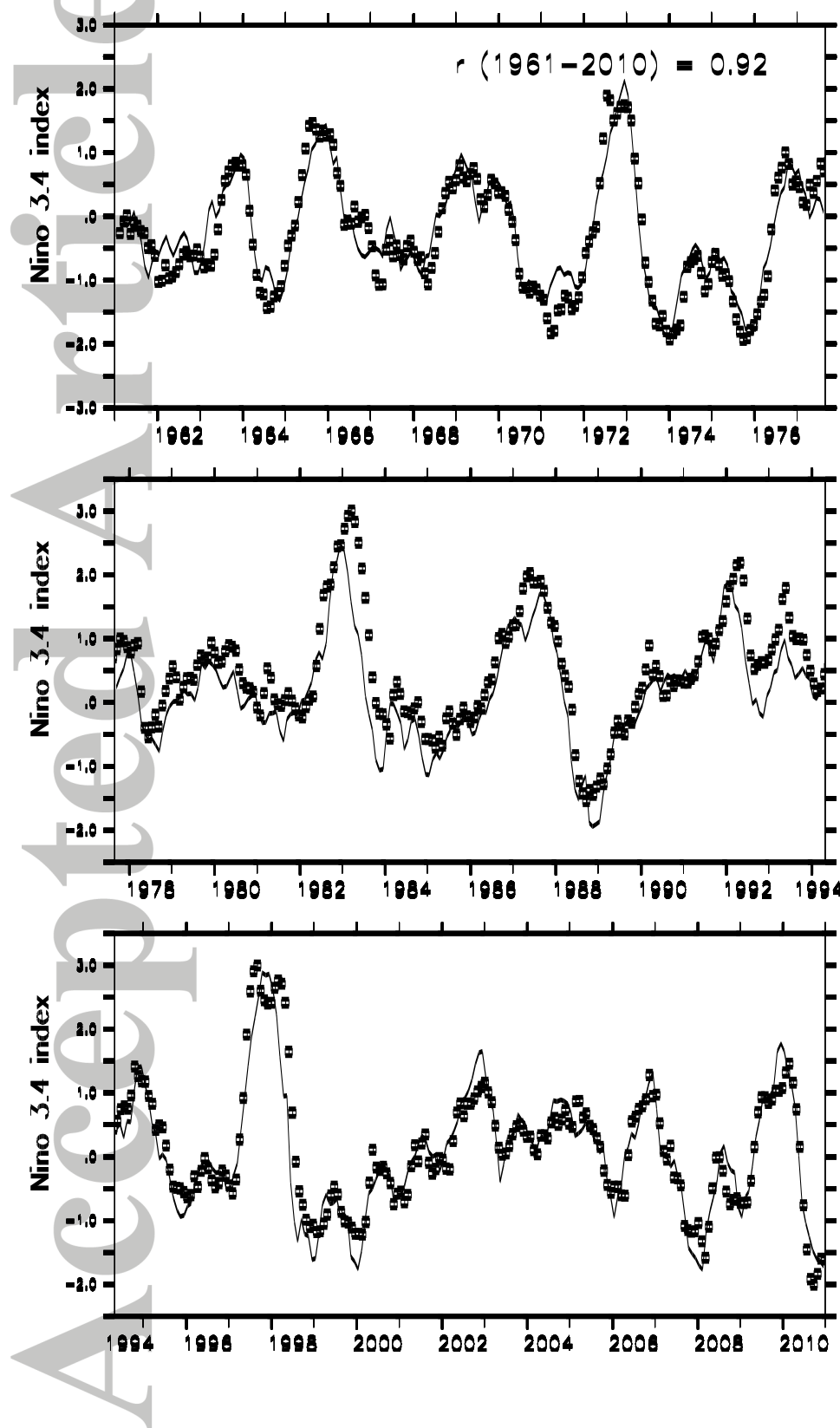


**Figure 1:** Normalized Niño 3.4 SST anomalies ( $170^{\circ}\text{W}-120^{\circ}\text{W}$ ,  $5^{\circ}\text{N}-5^{\circ}\text{S}$ ) from the ocean re-analysis data (full line) and that from the HadISST (boxes). Correlation between the two indices from 1961 to 2010 is 0.92. The high correspondence between two indices shows the fidelity of the ocean re-analysis.

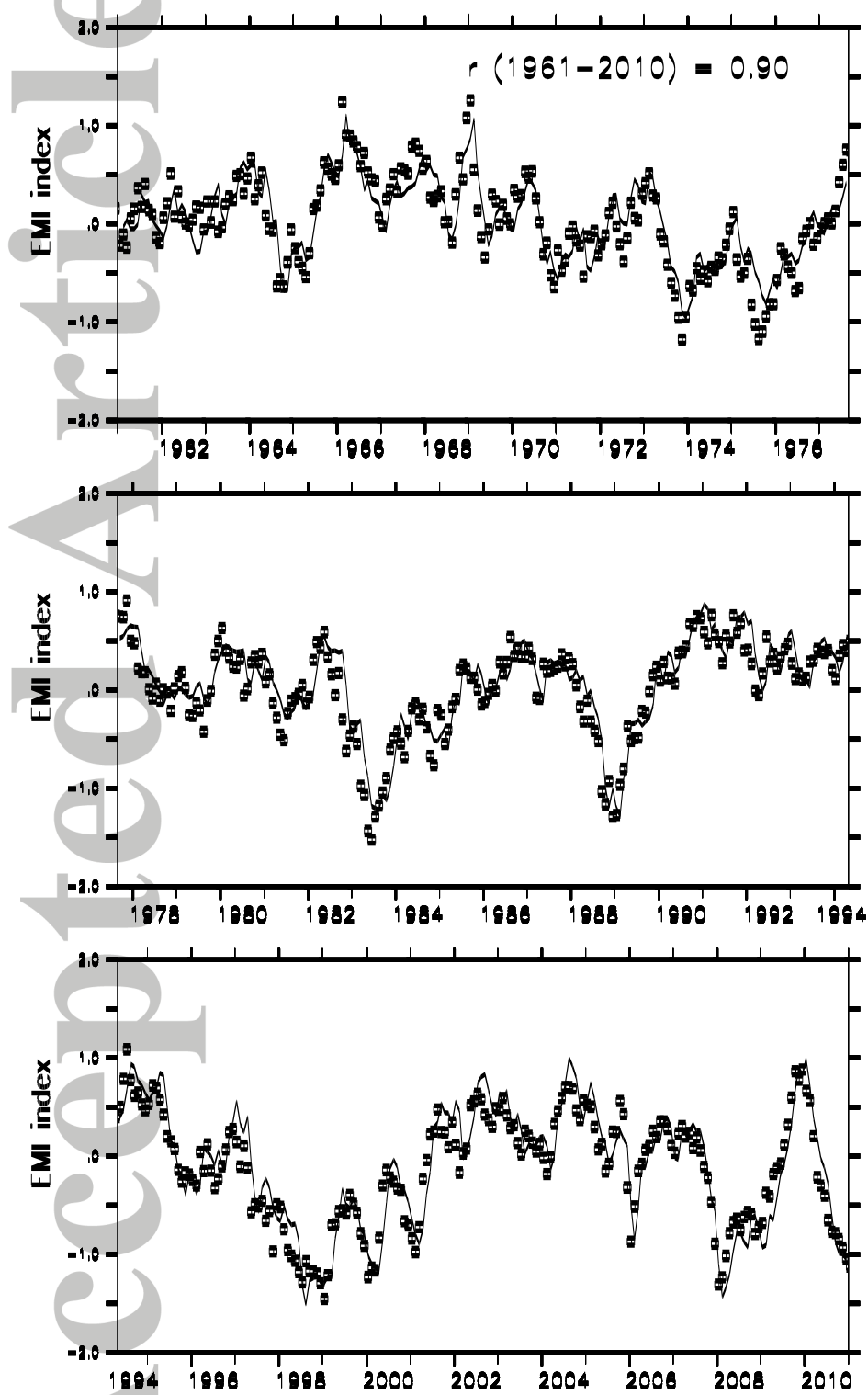


**Figure 2:** Same as previous figure but for El Niño-Modoki (EMI) index. EMI index is calculated as in Ashok et al., [2007]. Correlation between the indices is 0.9 over the entire period from 1960 to 2010.

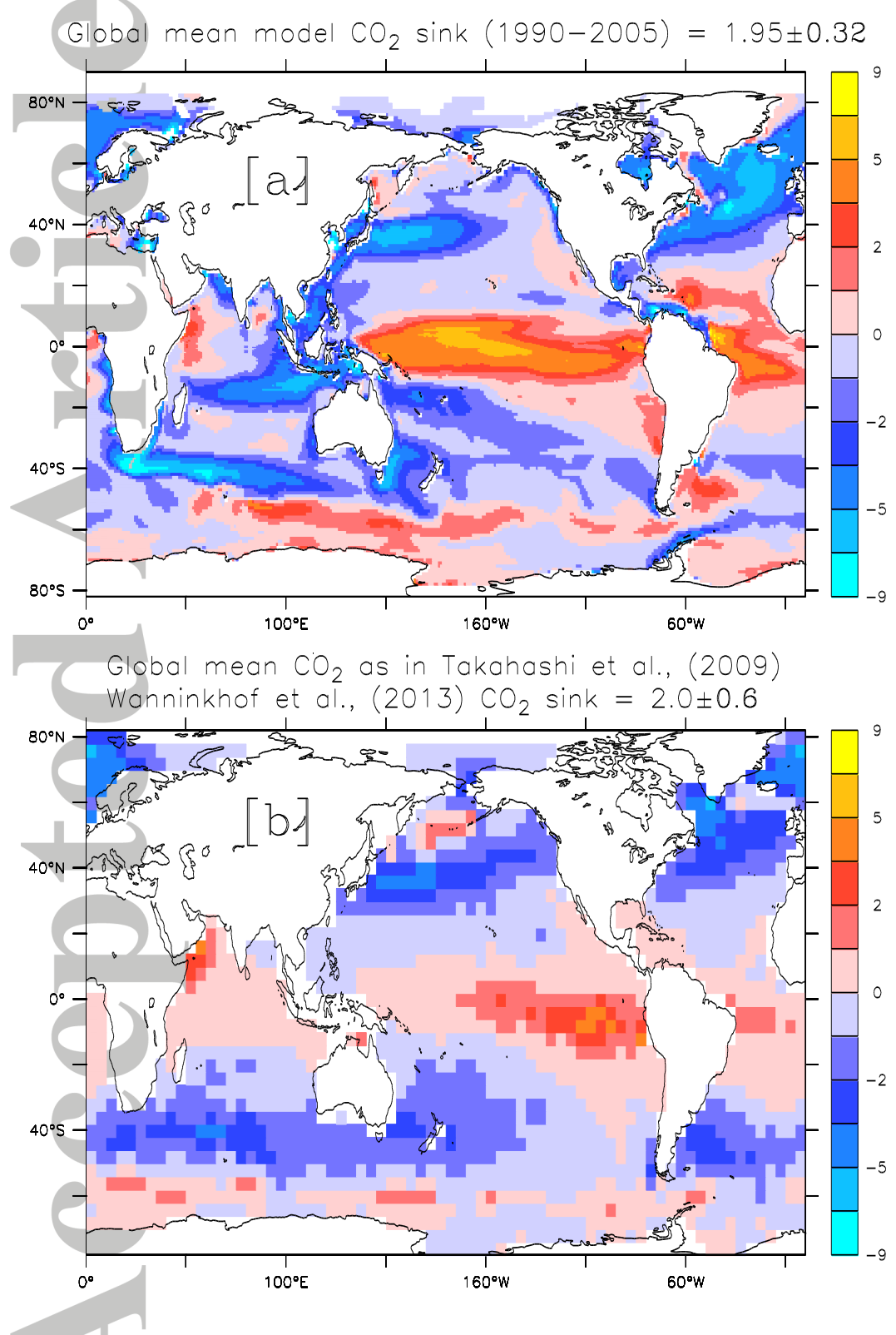


**Figure 3:** [a] 1990–2005 average of global ocean surface sea-to-air CO<sub>2</sub> fluxes from the model. Global total sink during this period is  $1.95 \pm 0.32$  PgC yr<sup>-1</sup>. [b] Sea-to-air CO<sub>2</sub> fluxes from Takahashi et al., [2009] database. Units are in moles m<sup>-2</sup> yr<sup>-1</sup>.

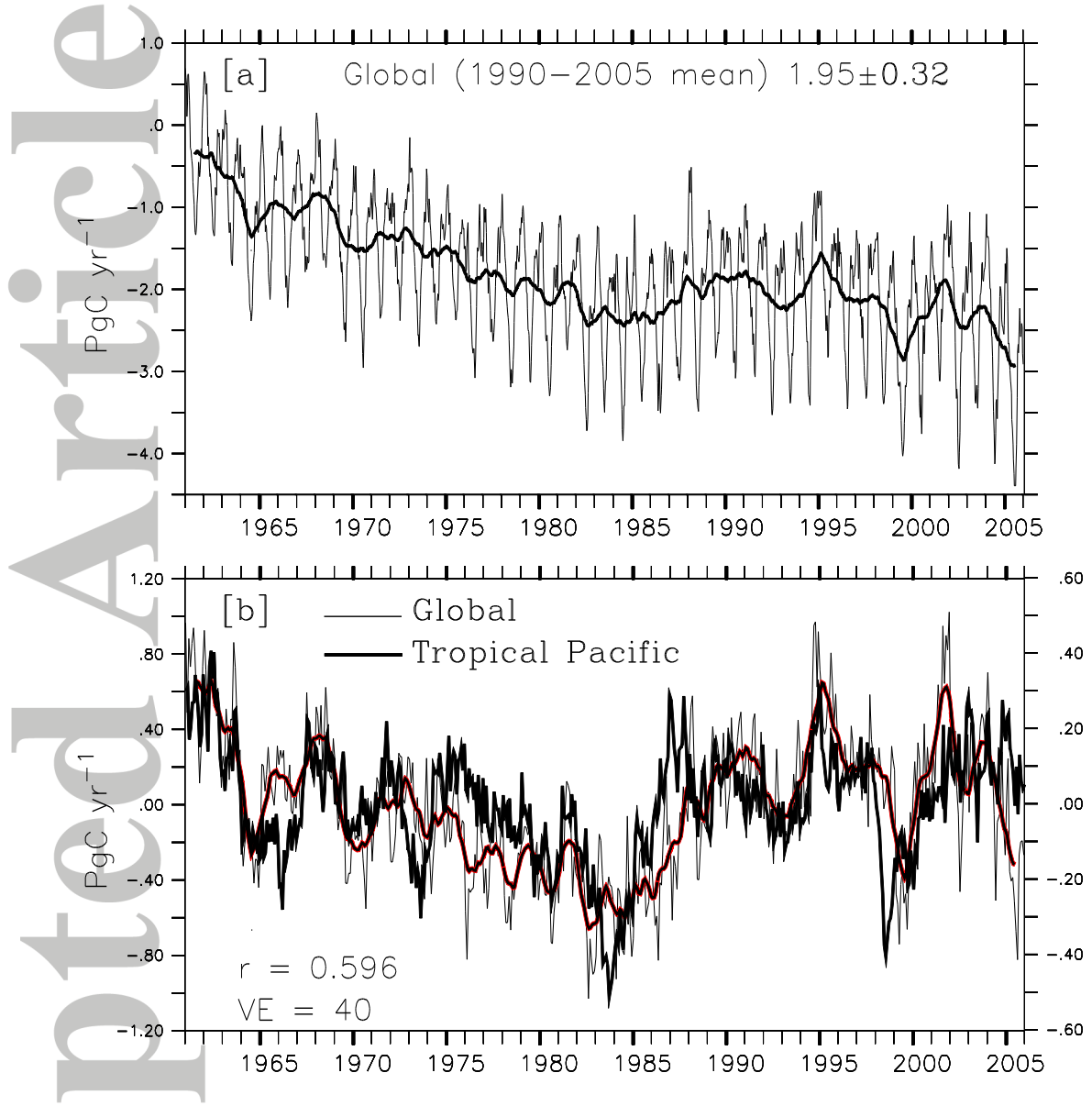


**Figure 4:** [a] Global integral of total sea-to-air CO<sub>2</sub> fluxes from 1961 to 2005 estimated by the model. [b] The model de-trended and de-seasonalized global total sea-to-air CO<sub>2</sub> flux anomalies (left axis) and corresponding tropical Pacific ( $160^{\circ}\text{E}-280^{\circ}\text{E}$ ,  $15^{\circ}\text{N}-15^{\circ}\text{S}$ ) flux anomalies (right axis). Tropical Pacific CO<sub>2</sub> flux anomalies are significantly correlated with global anomalies ( $r = 0.59$ ) and explain ~40% global anomaly variance. The thick red line is the 12-month running mean of global CO<sub>2</sub> flux anomalies.

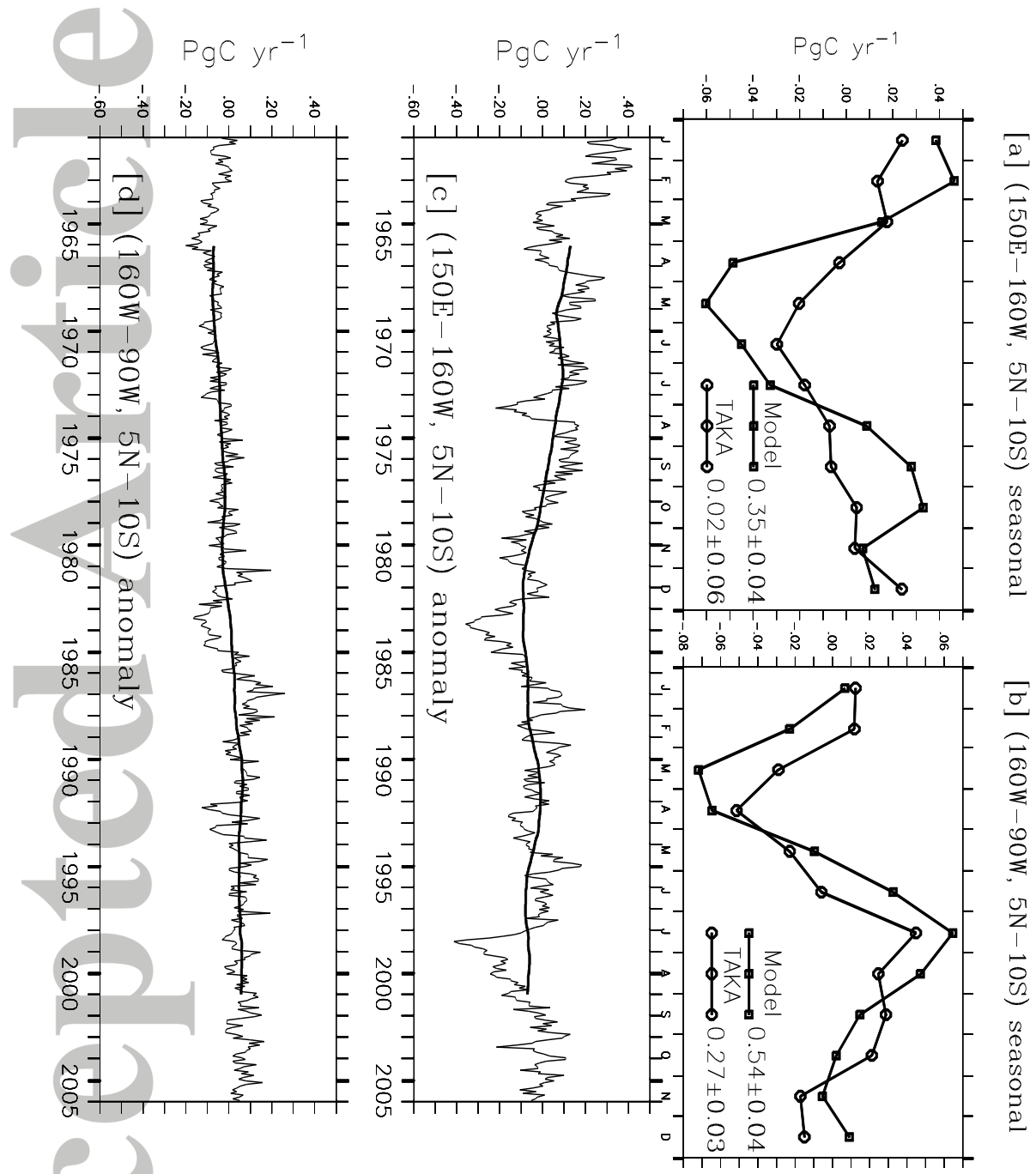


**Figure 5:** [a, b] Seasonal cycle of sea-to-air  $\text{CO}_2$  fluxes from western and eastern equatorial Pacific shown as comparisons between model and Takahashi et al., [2009]. [c, d] Interannual  $\text{CO}_2$  flux anomalies from the model integrated over western and eastern Pacific equatorial. The black lines show the 10-year running mean. All units are in  $\text{PgC yr}^{-1}$ .

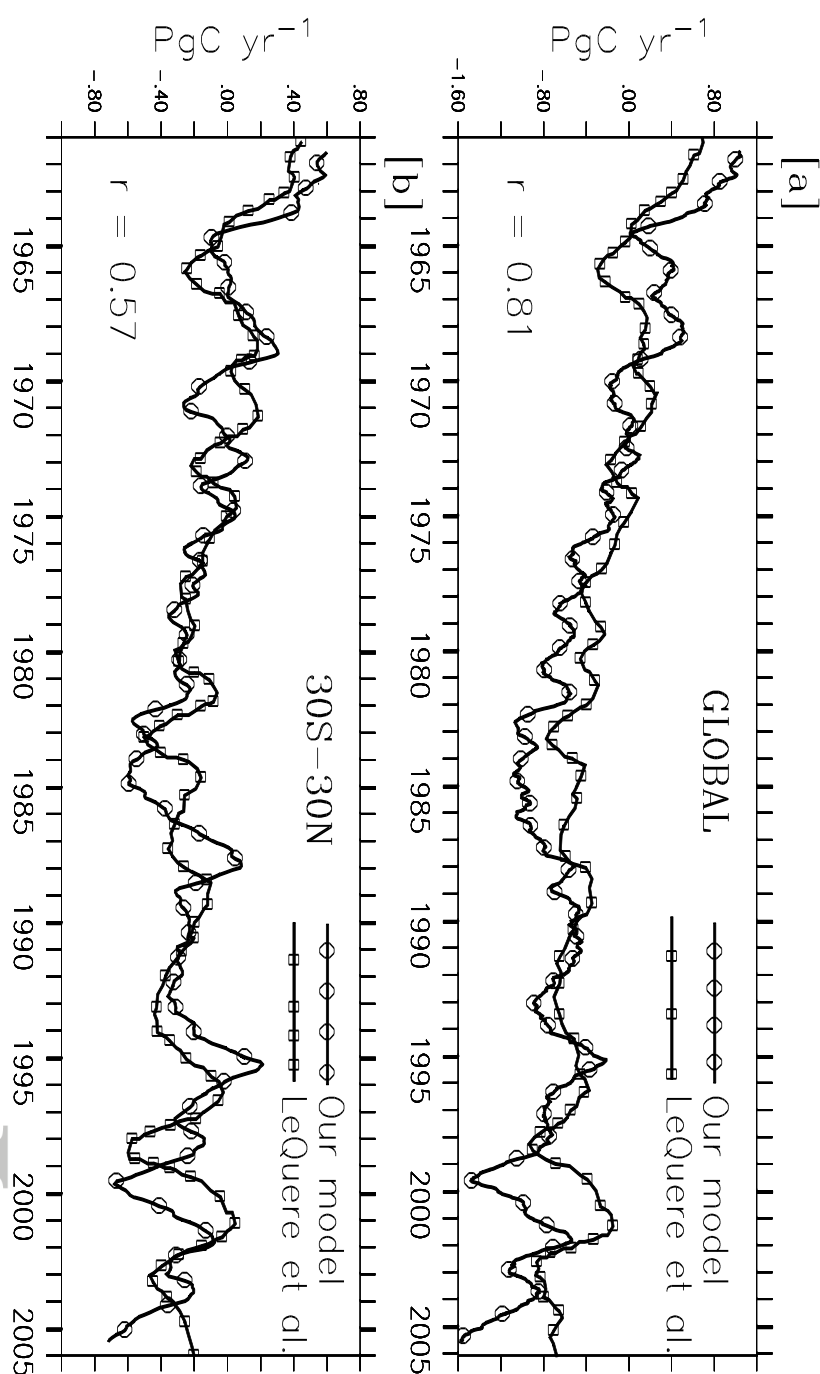


**Figure 6:** Comparison of [a] Global and [b] 30°S–30°N belt of ocean CO<sub>2</sub> flux anomalies between our model and LeQuere et al., [2010]. Correlations are given. Anomalies shown here are computed with respect to 1960–1981 climatological mean in order for the calculations to be consistent with Le Quere et al., [2010].

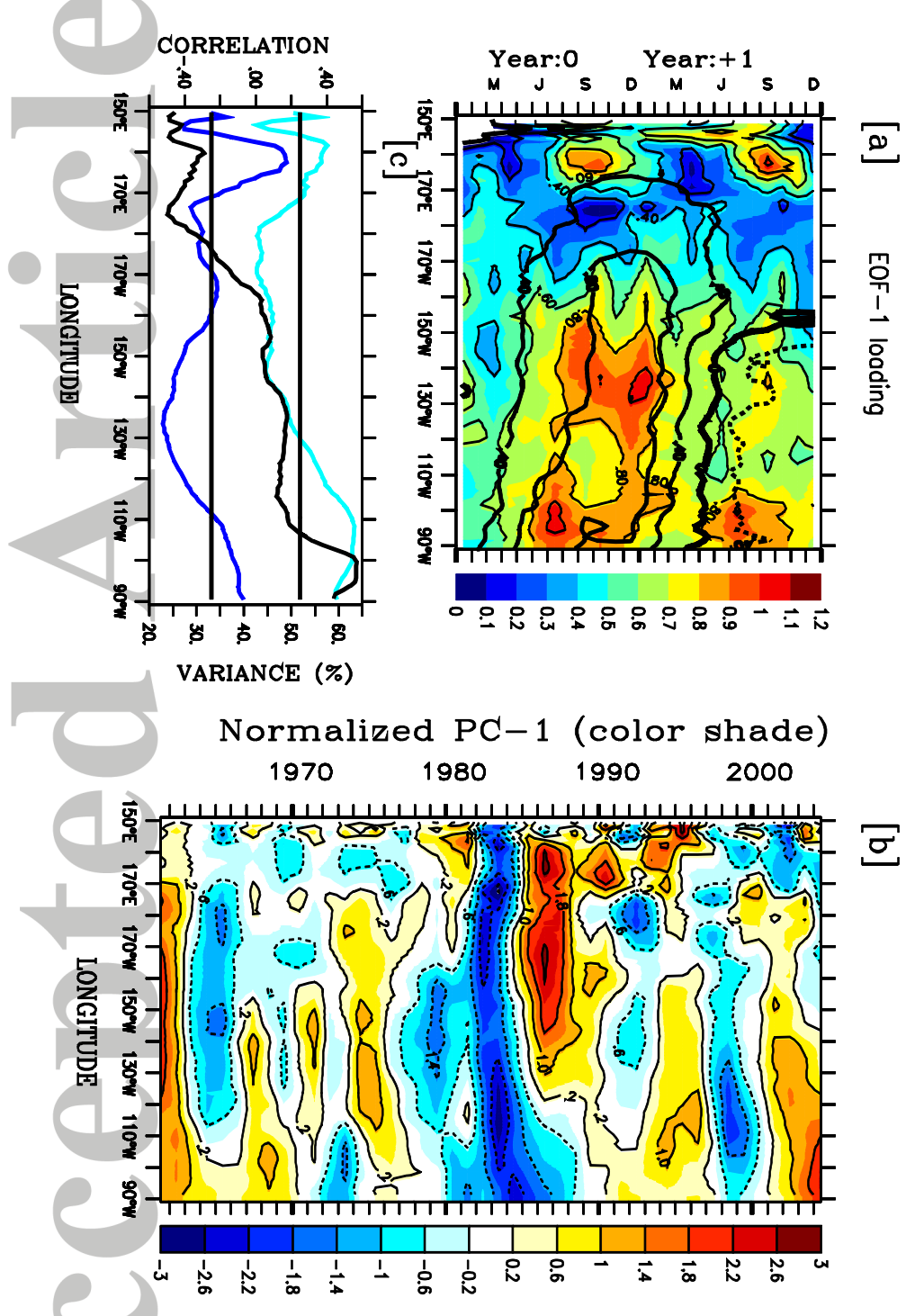


**Figure 7:** [a] Seasonal evolutions of the dominant mode of interannual variability (shown over two years; see text) of the equatorial Pacific CO<sub>2</sub> flux anomalies for each grid point from 160°E to 90°W (EOF-1, see section 2e for details). Colour shade represents CO<sub>2</sub> flux (moles m<sup>-2</sup> yr<sup>-1</sup>) and thick contour represents corresponding EOF-1 of sea surface temperature anomalies (SST; °C). [b] The principle components (PC-1; normalized) for each grid point from 160°E to 90°W. [c] Time-correlation between PC-1 and Niño 3.4 (blue) and El Niño-Modoki (cyan) from each grid point (left axis). The thick black line shows the variance explained by EOF-1 from each grid point (right axis).

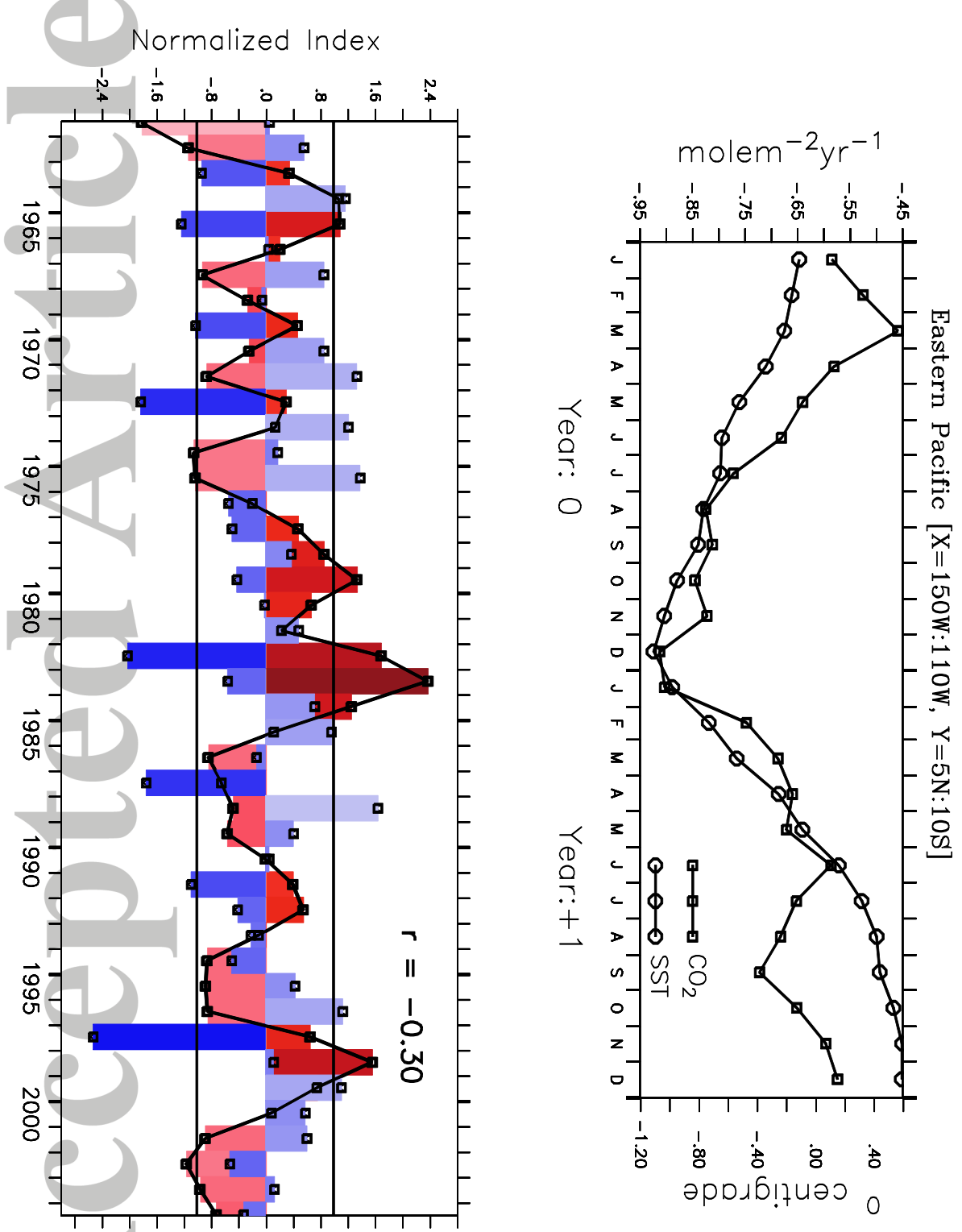


**Figure 8:** [a] Seasonal evolutions of the dominant interannual sea-air CO<sub>2</sub> flux anomalies (left axis) and SST anomalies (right axis) from the central-to-east Pacific (spatially averaged between 150°W-110°W in Figure-2) and shown for Year:0 and +1. [b] The PC-1 of CO<sub>2</sub> flux anomalies (red bars and thick black line) and SST anomalies (blue bars). EOF-1 and PC-1 of SST has been reversed in sign for easy comparison. The correlation coefficient between PC-1 of CO<sub>2</sub> flux and SST is shown.

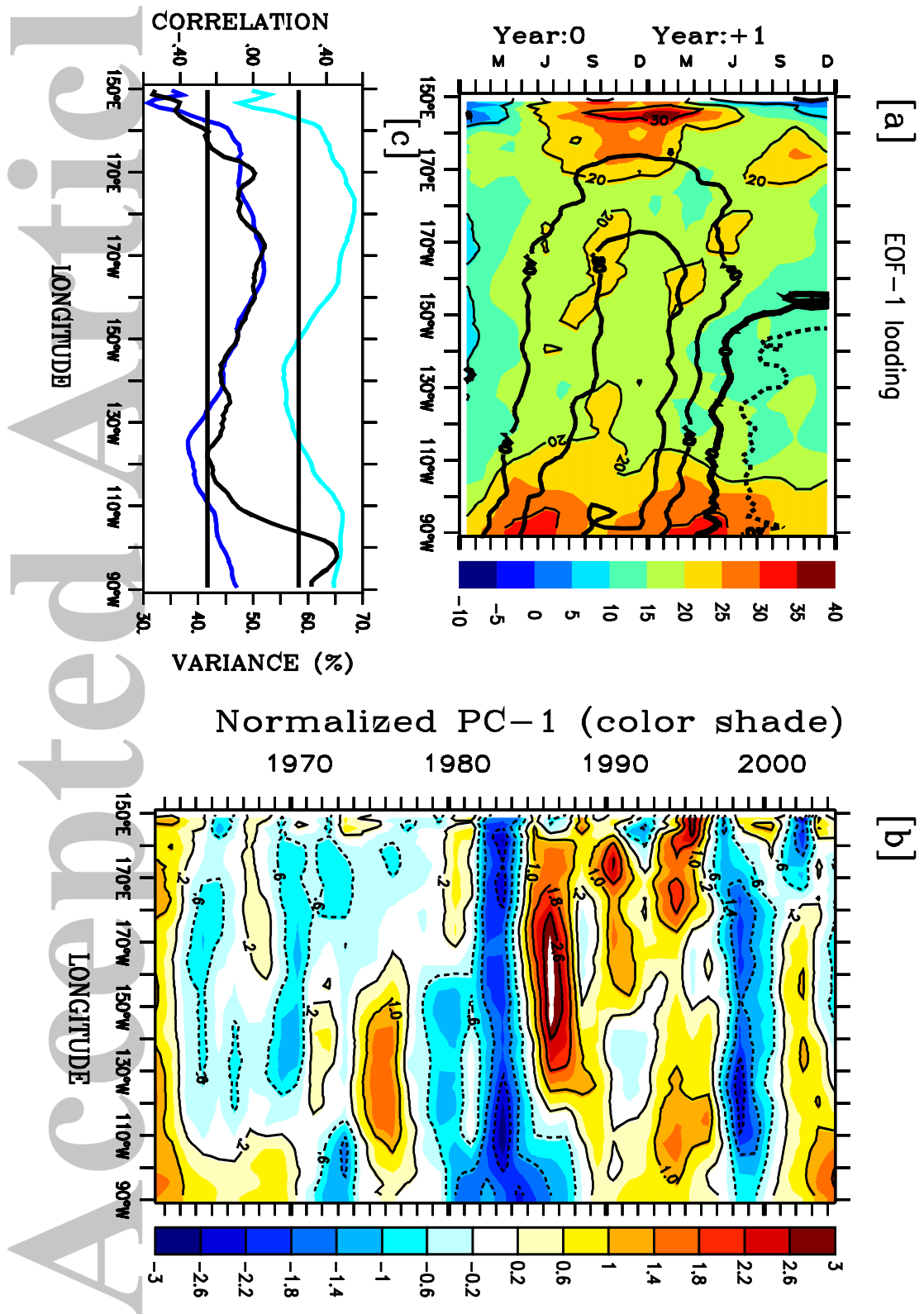


**Figure 9:** Same as Figure-7, but for pCO<sub>2</sub> anomalies (units are in  $\mu\text{atm}$ ).

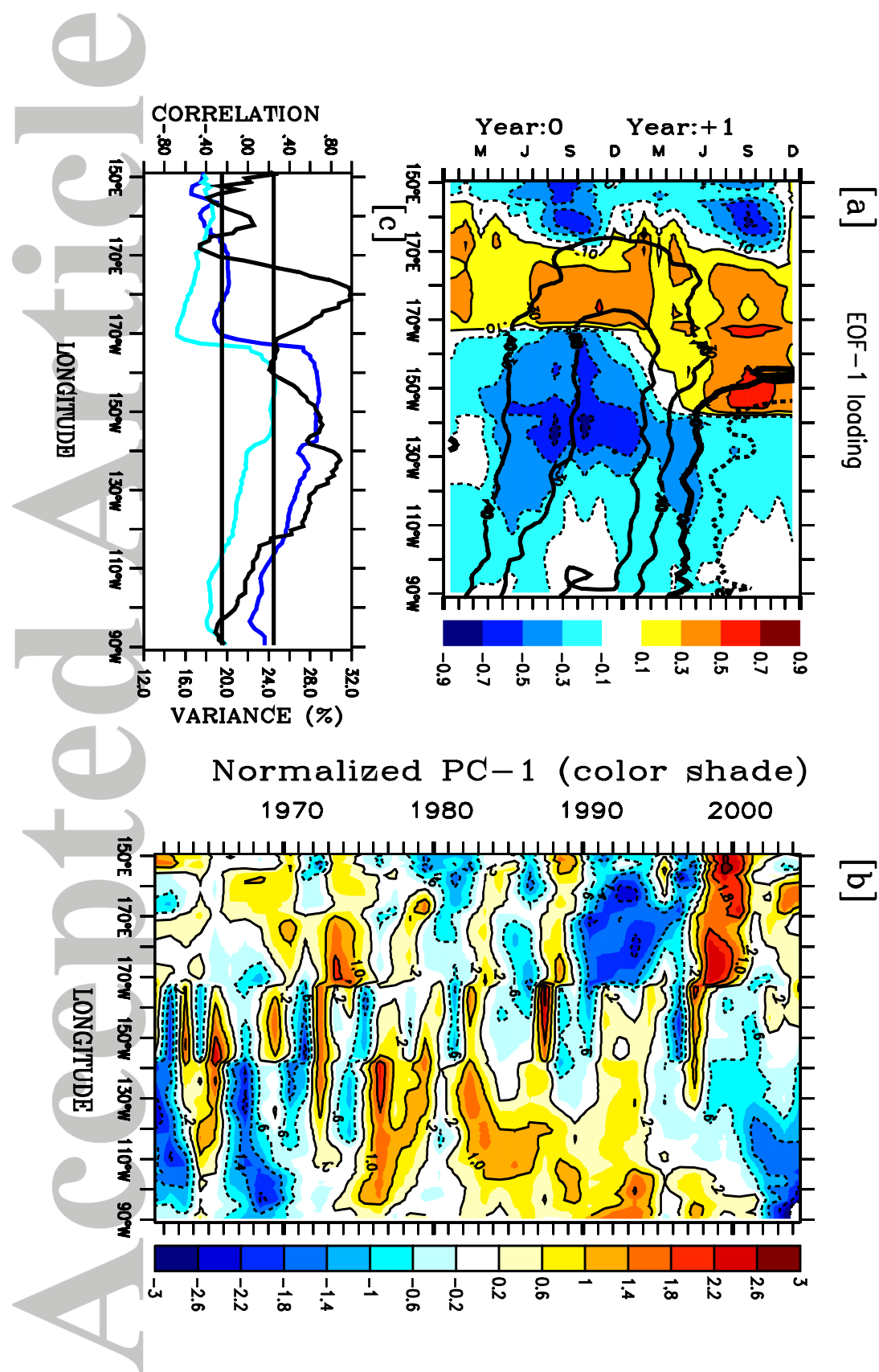


**Figure 10:** Same as Figure 7, but for CO<sub>2</sub> flux anomalies calculated as a difference between S3 and S4. The anomalies represent the effect of interannual variability in winds on CO<sub>2</sub> flux variability in the equatorial Pacific.

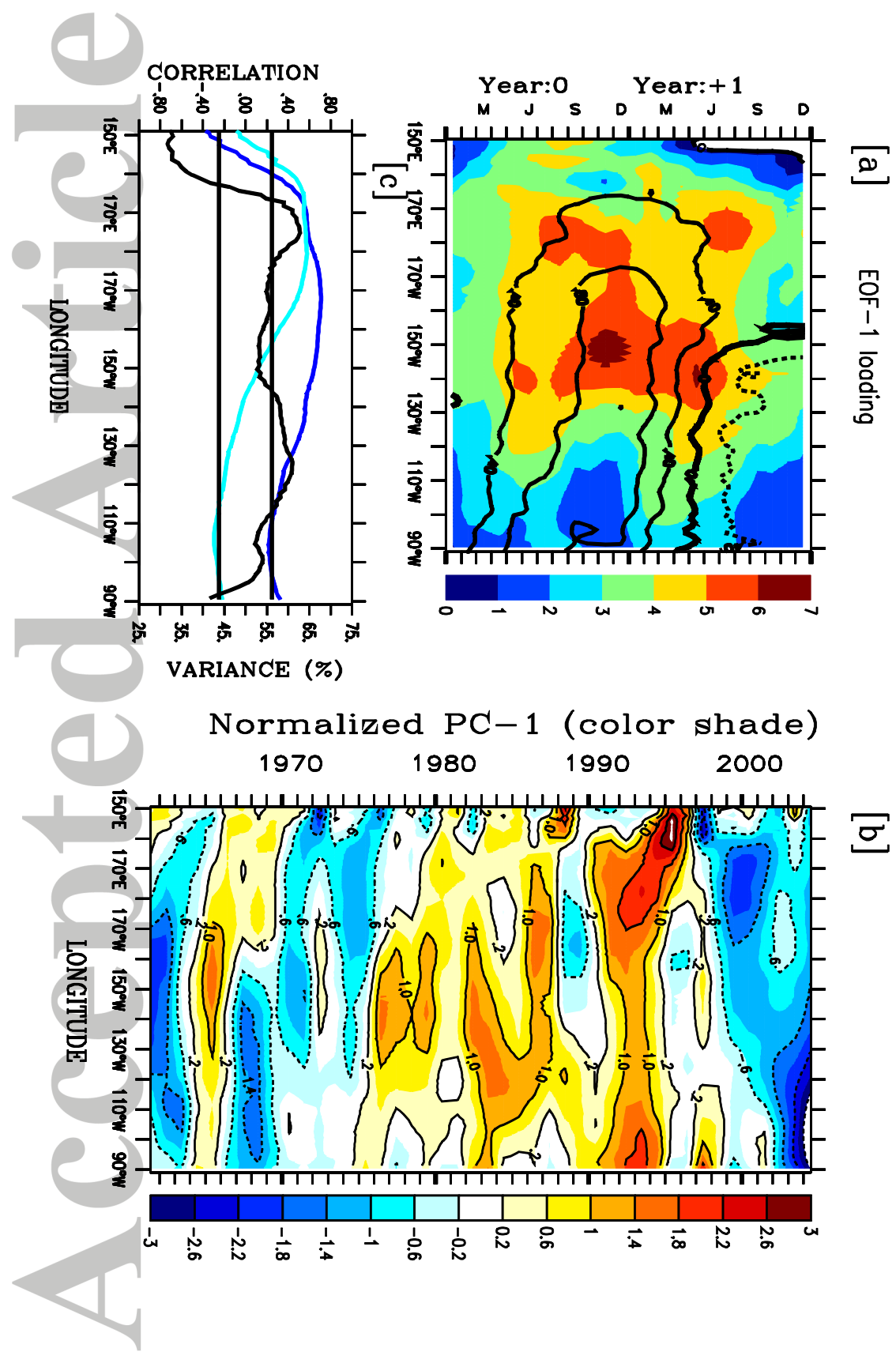


**Figure 11:** Same as Figure 10, but for pCO<sub>2</sub> anomalies.

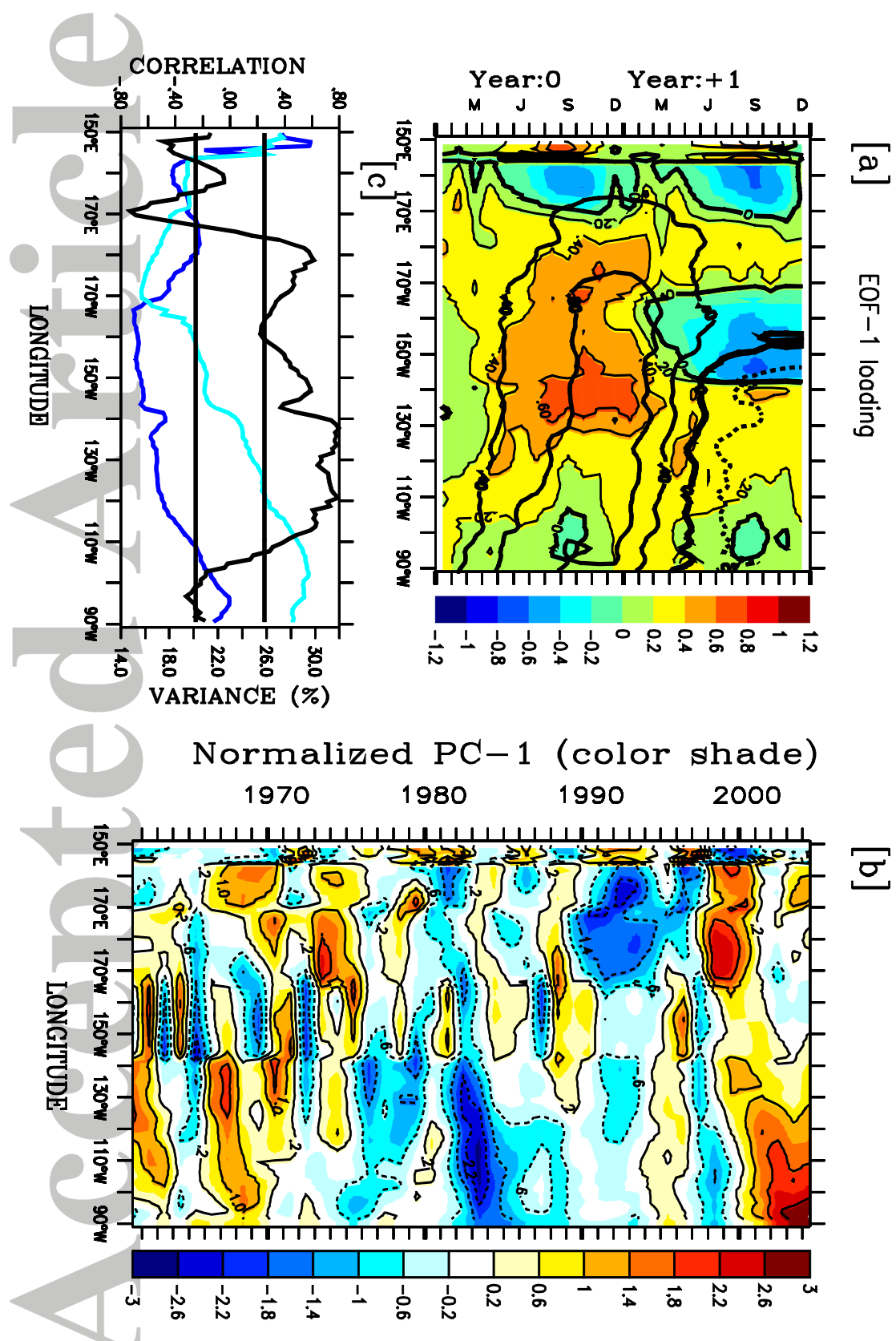


**Figure 12:** Same as Figure 10, but for CO<sub>2</sub> flux anomalies calculated as a difference between S3 and S5. The anomalies represent the effect of interannual variability in ocean dynamics on CO<sub>2</sub> flux variability in the equatorial Pacific.

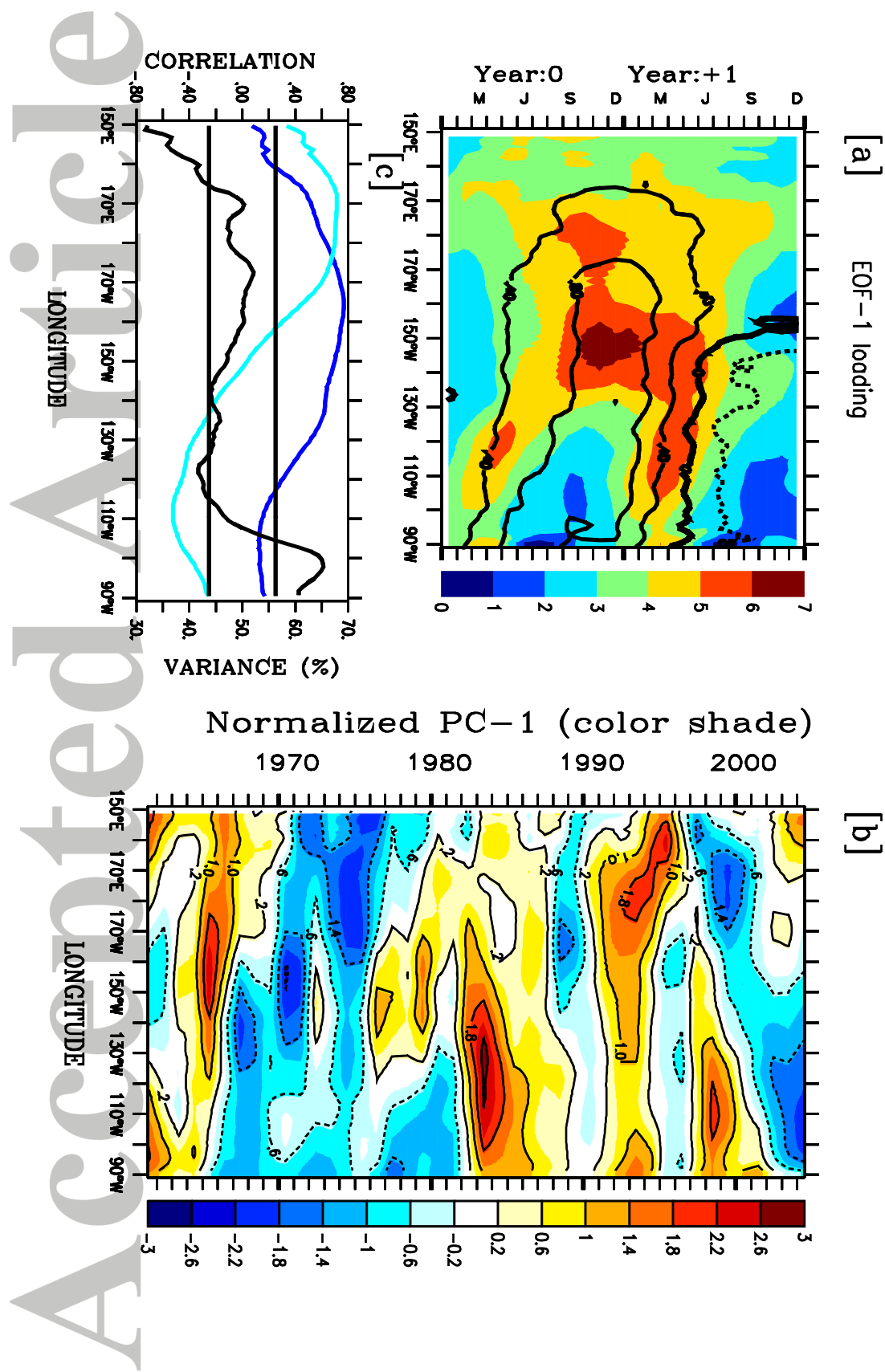


**Figure 13:** Same as Figure 12, but for pCO<sub>2</sub> anomalies.

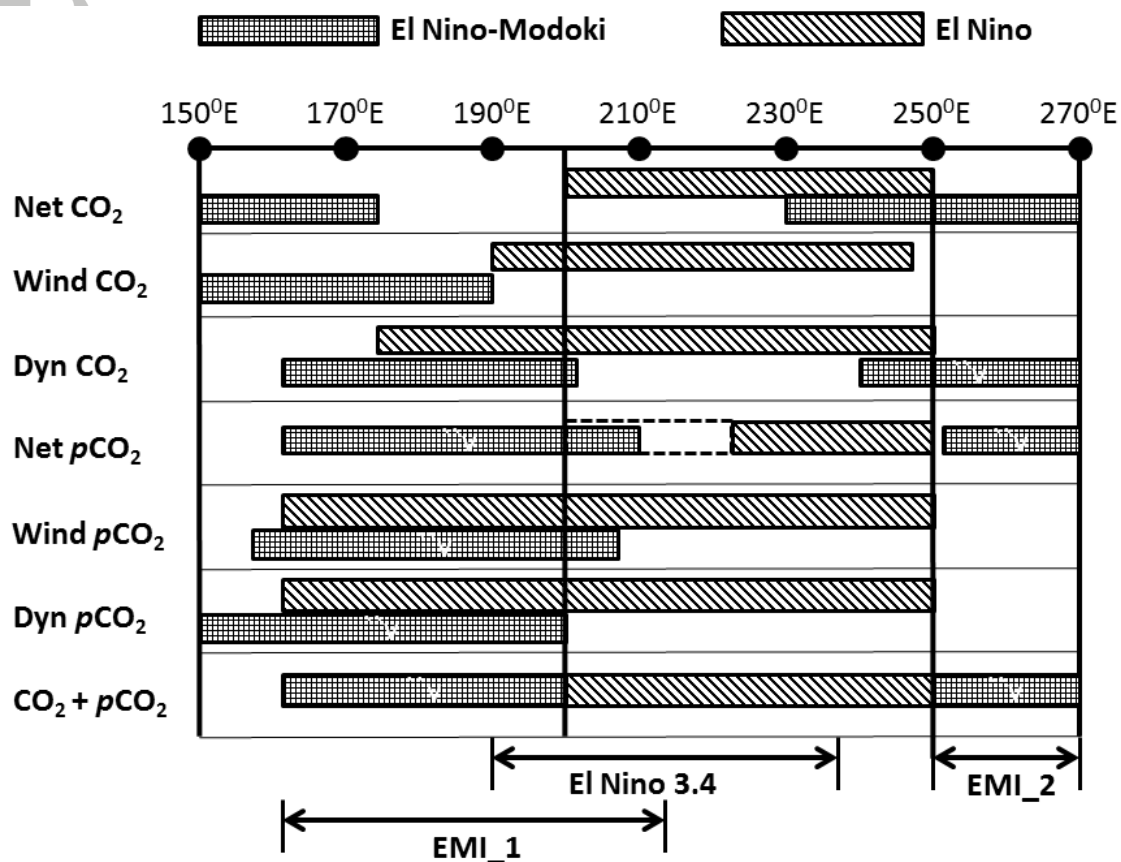


**Figure 14:** Summary of spatial coverages of dominant interannual variability of CO<sub>2</sub> fluxes and pCO<sub>2</sub> in the equatorial Pacific segregated according to regionally dominant mechanisms identified from Figure 7 through 13. Canonical El Niño is the dominant mechanism of carbon cycle variability in the central-to-east equatorial Pacific, nearly overlapping with the Niño 3.4 region. In the western (EMI\_1, 160°E-160°W) and far eastern (EMI\_2, 110°W-90°W) equatorial Pacific El Niño-Modoki is the dominant mechanism. The dashed box shows a region of model uncertainty in pCO<sub>2</sub>-ENSO relations. The y-axis just indicates the variable names.

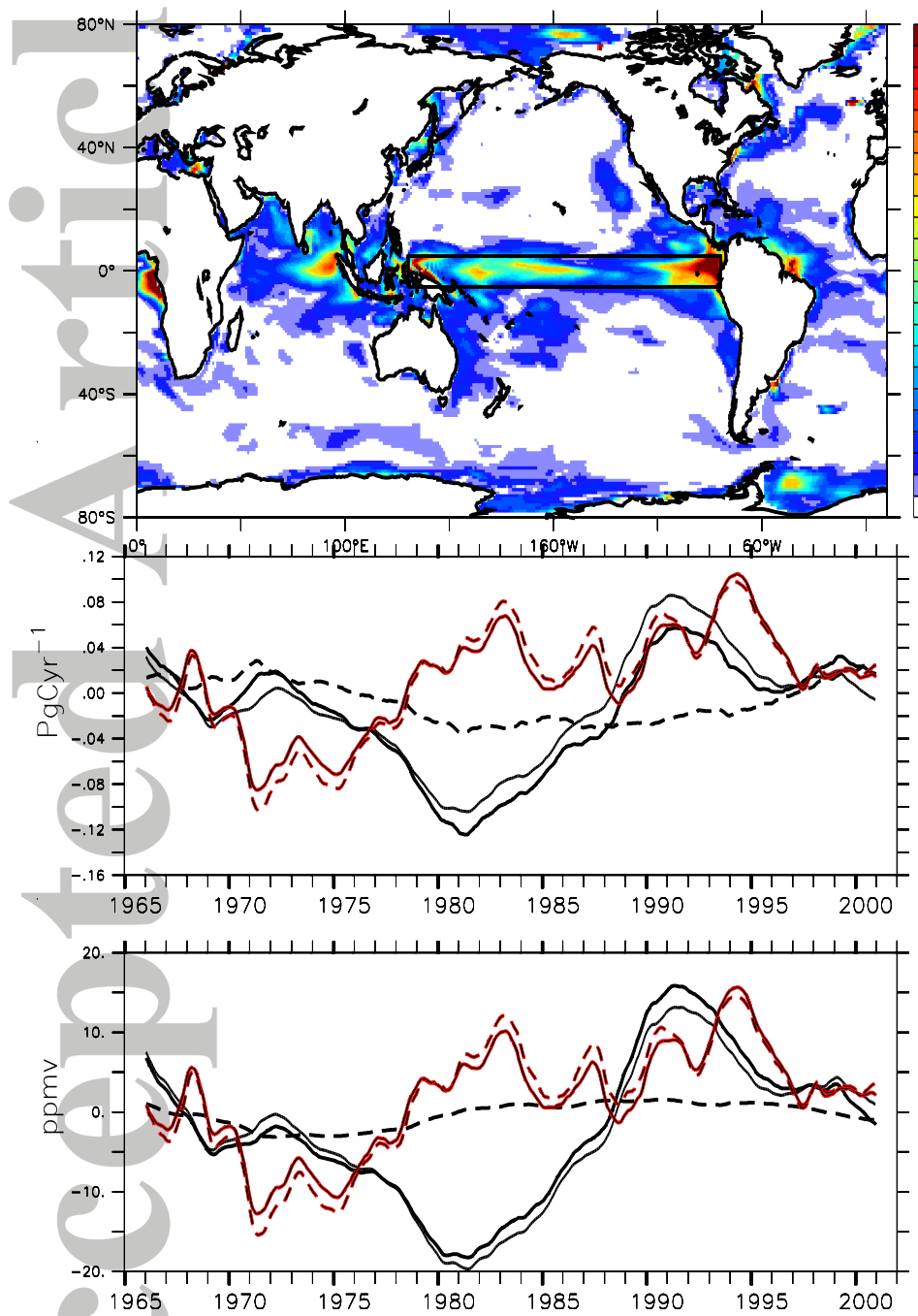


**Figure 15:** [a] Variance of 10-year smoothed pCO<sub>2</sub> anomalies calculated from 1961 to 2005 ( $\mu\text{atm}^2$ ). [b] Monthly CO<sub>2</sub> anomalies (de-trended and de-seasonalised) averaged over a box shown in (a) and smoothed by running mean over 10-years. Thick (thin) black line shows the CO<sub>2</sub> anomalies from S3 (S5) (see text for details). Thick dotted line shows the CO<sub>2</sub> anomalies from S4. The red lines show the SST anomalies averaged over the same box and smoothed by a 10-year running mean and scaled linearly to fit to the common y-axis. The solid (dashed) red lines show the SST anomalies from HadISST (GFDL re-analysis), respectively. [c] Same as (b) but for pCO<sub>2</sub> anomalies.

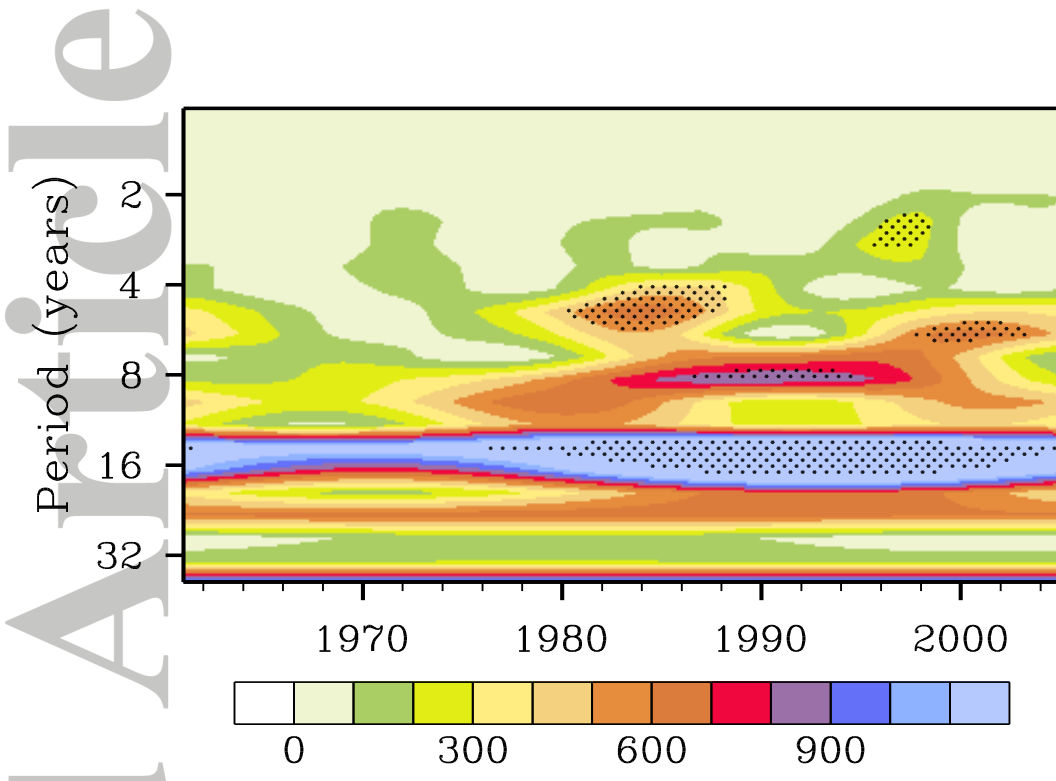


**Figure 16:** Wavelet power spectrum of the pCO<sub>2</sub> data shown in Figure 15c. The dots represent significance at 90% confidence level. Morlet wavelet is used and Fourier transform is performed [Torrence and Compo, 1998]. The wavelet power spectrum is defined as the absolute value squared of the wavelet transform and gives a measure of the time series variance at each scale (period) and at each time. Statistical significance is tested using Chi-square test.

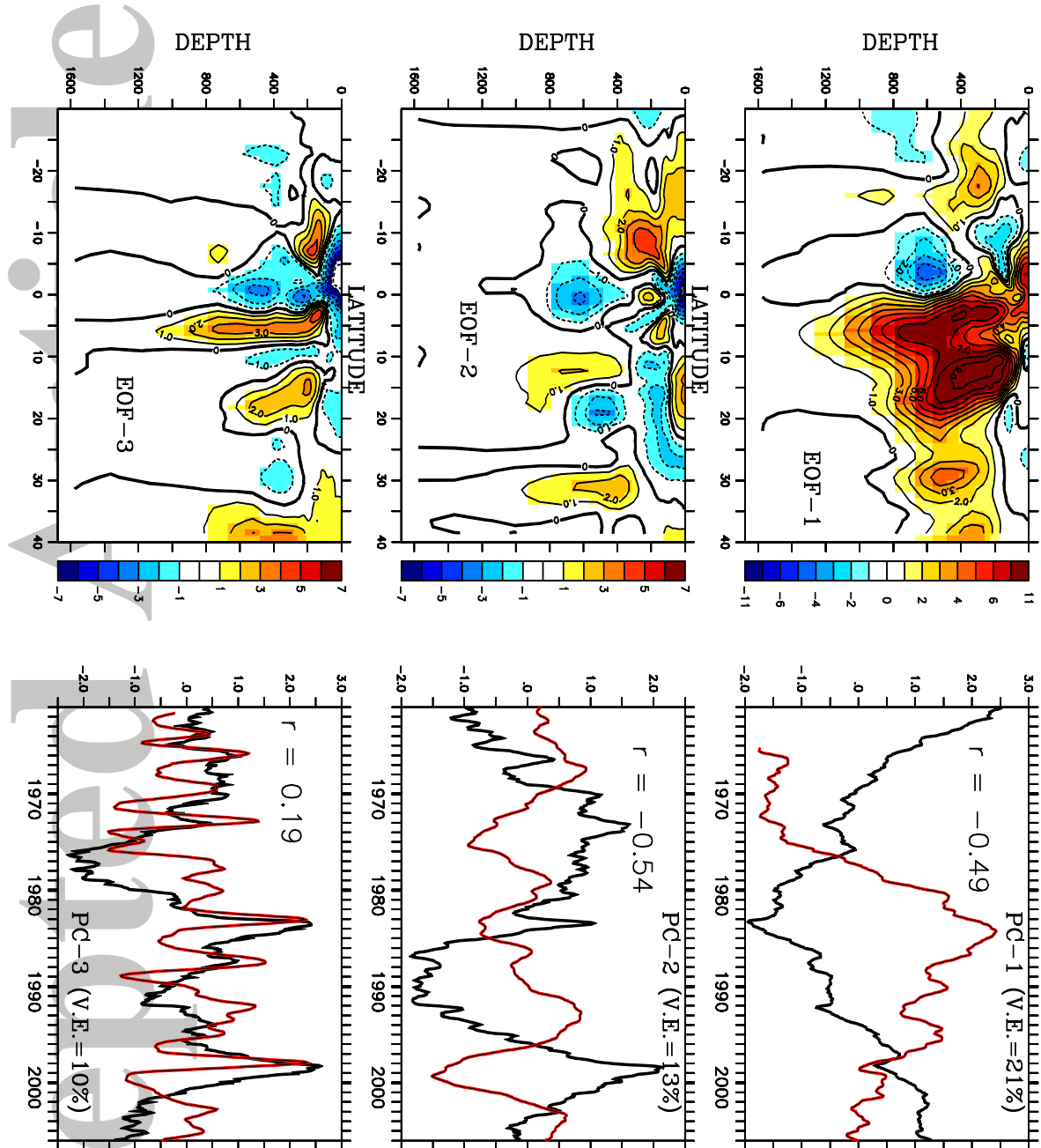


**Figure 17:** EOF-1 to 3 of dissolved inorganic carbon (DIC) anomalies (de-trended and de-seasonalised) computed over a latitude-depth section and averaged zonally over the Pacific longitudes from  $160^{\circ}\text{E}$ - $90^{\circ}\text{W}$ . Left panels show the EOF loadings and the right panels show corresponding principle components. The red lines in the right panels show the PDO index (10-year running mean), El Niño-Modoki index (2-year running mean) and El Niño index (1-year running mean) from top to bottom, respectively. EOF-1 explains the dominant decadal signal with 23% variance. EOF-2 explains the second dominant signal with 13% variance, and EOF-3 shows the El Niño variability with 10% variance. EOF loadings are in  $\mu\text{mole kg}^{-1}$  and all PCs and climate indices are normalized.